AD-A216 248

A WIND TUNNEL STUDY OF A

STING-MOUNTED CIRCULATION CONTROL WING

THESIS

JOHN W. TRAINOR
CAPTAIN, USAF

AFIT/GAE/ENY/89D-38

DEPARTMENT OF THE AIR FORCE

AIR UNIVERSITY

AIR FORCE INSTITUTE OF TECHNOLOGY

Wright-Patterson Air Force Base, Ohio

89 12 29 038

A WIND TUNNEL STUDY OF A

STING-MOUNTED CIRCULATION CONTROL WING

THESIS

JOHN W. TRAINOR
CAPTAIN, USAF

AFIT/GAE/ENY/89D-38

DTIC
ELECTE
JAN 0 2 1990
S
B
D

AFIT/GAE/ENY/89D-38

A WIND TUNNEL STUDY OF A

STING-MOUNTED CIRCULATION CONTROL WING

THESIS

Presented to the Faculty of the School of Engineering

of the Air Force Institute of Technology

Air University

In Partial Fulfillment of the

Requirements for the Degree of

Master of Science in Aerospace Engineering

John W. Trainor, B.S.

Captain, USAF

December, 1989

Acknowledgements

I have many individuals to recognize for their contributions to this, my first research effort. Thanks are due to my research advisor, Dr. Milton Franke, and to my research committee members, Col Paul King and Capt Phil Beran, for their counsel and direction. From the AFIT aero labs, Mr. Nick Yardich, Mr. Dan Rioux, and Mr. Andy Riemenschneider provided invaluable assistance with instrumentation and tunnel operation. Without the skilled workmanship of Mr. Dave Driscoll, who provided the experimental model, this study would not have been possible. I am especially grateful to Mr. Steve DeCook, friend and fellow student, for taking time from his own studies to troubleshoot difficulties with data acquisition software. Finally, I express my deepest appreciation to my wife Lisa, not only for her unending encouragement, but more importantly for providing stability and perspective in my life during an often trying experience.

Accession For	
NTIS GRA&I	☑
DTIC TAB	☐
Unannounced	☐
Justification	
By	
Distribution/	
Availability Codes	
Dist	Avail and/or Special
A-1	

ii

Table of Contents

List of Figures

List of Tables

List of Symbols

A	area (ft^2)
AX	axial force (lb_f)
b	wing span (ft)
b_s	slot span (ft)
c	wing chord (ft)
C	path of integration
C_d	Venturi coefficient of discharge
C_D	wing drag coefficient
C_{DE}	wing equivalent drag coefficient
CG	center of gravity
C_ℓ	section lift coefficient
C_L	wing lift coefficient
C_{Mle}	pitching moment coefficient
C_p	pressure coefficient
$C\mu$	momentum coefficient
$C0$	offset coefficient (lb_f/in^2)
$C1$	sensitivity coefficient $[lb_f/(in^2\text{-volt})]$
$C2$	nonlinearity coefficient $[lb_f/(in.^2\text{-volt}^2)]$
d	section drag (lb_f/ft)
ds	differential length
D	wing drag (lb_f)
D_E	wing equivalent drag (lb_f)
h	slot height $(in.)$
k	ratio of specific heats for air
ℓ	rolling moment element $(in.\text{-}lb_f)$

viii

ℓ	section lift (lb_f/ft)
L	wing lift (lb_f)
$\dot{m}$	mass flow rate (slugs/s)
M	Mach number
$N1$	normal force element 1 (lb_f)
$N2$	normal force element 2 (lb_f)
P	pressure, absolute (lb_f/ft^2)
q	dynamic pressure (lb_f/ft^2)
r	Coanda surface radius (in.)
R	gas constant for air $[ft^2/(s^2\text{-deg R})]$
Re	Reynolds number, $\rho_\infty v_\infty c/\mu$
S	wing planform area (ft^2)
T	temperature (deg R)
v	velocity (ft/s)
V	volts
x	chordwise wing dimension (ft)
y	spanwise wing dimension (ft)
Y	compressibility factor
$Y1$	side force element 1 (lb_f)
$Y2$	side force element 2 (lb_f)
z	airfoil dimension normal to chord (ft)
α	wing geometric angle of attack (deg)
Γ	circulation (ft^2/s)
ρ	density of air $(slugs/ft^3)$
Θ	trailing edge angle (deg)
μ	coefficient of viscosity of air $(lb_f\text{-s}/ft^2)$

Subscripts

$(\ )_{atm}$ atmospheric conditions

$(\ )_j$ jet conditions

$(\ )_t$ plenum stagnation conditions

$(\ )_1$ conditions upstream of Venturi

$(\ )_2$ conditions at Venturi throat

$(\ )_\infty$ free-stream conditions

Abstract

This wind tunnel study investigated the feasibility of testing a sting mounted circulation control wing. A 20% thick, 8.5% cambered rectangular wing was designed, built, and tested in the AFIT 5-ft wind tunnel. Lift, drag, equivalent drag, and pitching moment coefficients were obtained at Reynolds numbers of 6×10^5 and 9×10^5. The force and moment results achieved indicate supercirculation was not present. Flow visualization with nylon tufts displayed extreme flow disruption at the trailing edge, due to free-stream impingement on both the sting and blowing air supply hoses. The available blowing air supply was not strong enough to produce a jet flow with the momentum needed to overcome this disruption. Wing model design changes were recommended to alleviate this problem.

xi

A WIND TUNNEL STUDY OF A
STING-MOUNTED CIRCULATION CONTROL WING

I. Introduction

Background

The study of VSTOL technology continues to be one of the most promising and exciting disciplines of aeronautical research. In this era of fiscal deficits and shrinking budgets, both military and commercial aviation stand to benefit from advances in VSTOL technology. With modern stand-off weapons rendering any airfield vulnerable to severe battle damage, VSTOL vehicles offer basing flexibility and usage of austere airstrips to the military. Space and noise limitations on metropolitan airports necessitate low speed, steep descent commercial aircraft. Both military and commercial aviation benefit from performance advantages, such as higher lift at lower angles of attack, higher payloads, greater fuel economy, etc. With these and other inherent advantages, VSTOL technology is poised to play an ever increasing role in worldwide aviation.

The collective VSTOL field includes a multitude of lift augmentation techniques, one of which is circulation control. The Kutta-Joukowski theorem states that the lift generated by an airfoil is proportional to a quantity called

1

circulation. Circulation, Γ, is defined as

$$\Gamma = \oint_C \vec{v} \cdot \vec{ds} \qquad (1)$$

where $\vec{v} \cdot \vec{ds}$ is the scalar product of the velocity vector and the differential vector length along the path of integration, C. For an airfoil, $\vec{v} \cdot \vec{ds}$ represents the velocity component tangential to the airfoil surface; C is the closed curve representing the airfoil. By increasing this circulation, one obtains a direct increase in the lift of an airfoil.

The technique of circulation control attempts to increase this circulation through the Coanda effect which, simply put, is the ability of a high-energy jet to flow around a blunt surface without separation. This effect is generally attributed to a balance between the centrifugal force of the jet and the reduced static pressure on the blunt surface due to the jet velocity (1:2). Circulation control airfoils employ this effect by introducing a high-energy jet onto the upper, trailing-edge region of a blunt trailing-edged airfoil (occasionally, leading-edge blowing is also used). Figure 1 is an illustration of a typical circulation control airfoil. At relatively low blowing rates, this jet re-energizes the boundary layer, allowing the flow to negotiate the blunt trailing edge without separation. This results in a reduced pressure drag and a somewhat enhanced lift. Increasing the blowing rate forces both the fore and aft stagnation points onto the airfoil

Pressure-Centrifugal
Force Balance

V_∞

P_∞

$P > P_\infty$

V_j

Jet Sheet
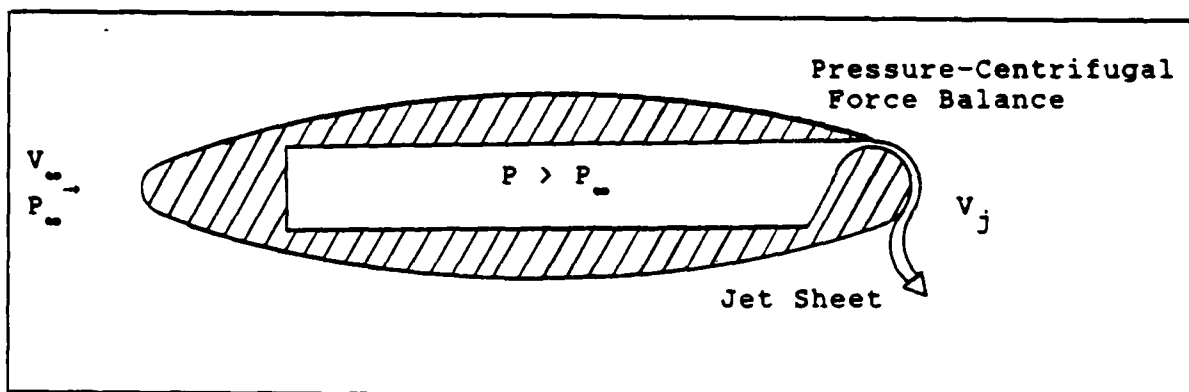
Figure 1.   A Typical Circulation Control Airfoil

lower surface, directly increasing the circulation and hence

the lift.   This condition is called supercirculation (1:2).

The most obvious advantage of circulation control is

the ability to vary lift by changing blowing rates; no angle

of attack change is necessary. Also, weight and mechanical

complexity is reduced over the conventional flap.   Drawbacks

include increased pressure drag at cruise; power required to

maintain blowing; large nose-down pitching moment; and

losses due to jet/free-stream mixing (2:737).

Previous Research

Circulation control is not a new concept; indeed, a

large data base of experimental research exists.   Kind &

Maul (3:170-182) achieved lift coefficients exceeding 3.0

with an elliptic airfoil, proving circulation control to be a bona fide high lift technique. Later, Englar (4), Williams & Howe (5), and Abramson (6), in particular, made great strides in understanding and documenting circulation control effects for various airfoil/trailing-edge geometries. Collectively, their major findings include:

- Greatest Coanda jet turning with a circular trailing edge.
- Nearly linear relation between C_l and V_j/V_∞.
- Center of pressure located approximately mid-chord.
- Low free-stream Re, high slot height detrimental to lift capability.

In addition, Loth (7) and Englar (8) independently modified demonstrator aircraft with circulation control wings. Both aircraft flew limited test profiles as a feasibility demonstration of full scale circulation control lifting surfaces.

Considerable circulation control research has been accomplished at AFIT (9:1-27). Single slot blowing, dual slot blowing, and splitter plate effects were experimentally studied. All else being equal, dual slot blowing was found to be more effective than single slot blowing at equivalent blowing momentum coefficients (defined later). Maximum l/d was obtained by limiting primary (upstream) slot blowing to just that needed to maintain flow attachment up to the

secondary slot. A fixed splitter plate improved airfoil performance over most conditions.

Recently, numerical modelling of 2-D circulation control has been attempted, with limited success. Various modelling techniques, including discrete vortices, Navier-Stokes solvers, and boundary layer stability theory have been examined. The viscous interactions of free-stream/blown jet mixing is most challenging to model and solve; no one method has proven completely reliable. As in all aeronautical research, however, increasingly powerful computers with more robust numerical techniques will eventually augment experimental testing of circulation control concepts. AFIT contributions to this field include a masters thesis by Williams (10). Reference 11 provides a collection of some of the more recent numerical/analytical research within both government and industry.

Present Study

Prior to this study, no research on sting-mounted circulation control models had been conducted at AFIT. This study investigated the feasibility of testing a sting-mounted circulation control wing, with quality of test results determined primarily by a comparison with 2-D data achieved by Harvell (12). Harvell designed and tested an 8.5% cambered, 20% thick section with two trailing-edge slots. This section incorporated the basic geometry of two airfoils previously tested by Englar (1). The most aft slot was located on a cylindrical trailing edge and was rotated

5

to any desired location. Testing with this model confirmed that dual slot blowing generated greater lift coefficients than single slot blowing under some conditions. Operationally, this leads to reduced blowing requirements and corresponding reductions in weight and power required.

To conduct the present study, a 3-D, sting-mounted, circulation control wing was designed with Harvell's basic section. Wind tunnel tests were performed in the AFIT 5-ft wind tunnel at Reynolds numbers (Re) of 6×10^5 and 9×10^5.

Research Objective

The sting balance/data acquisition system is a relatively new asset to the AFIT 5-ft wind tunnel facility. Prior to this test, no blown wing research had been accomplished with this system. Accordingly, the objective of this research was to design, build and test a fully 3-D circulation control model, utilizing this new system. In addition, a new pressure scanning system has been added to the facility. The model was pressure tapped, and pressure data were acquired with this new system to ascertain spanwise flow uniformity and Coanda turning effectiveness.

II. Test Item Description and Instrumentation

Wing

The experimental model (Figure 2) was a 20-percent thick, 8.5-percent cambered, rectangular wing with two tangentially blowing slots. It encompassed the basic elliptical section tested by Harvell (Figure 3), with slight modifications to the trailing edge and internal plumbing.

Planform sizing came under several constraints. First, the sting balance normal and axial force limits are 200 lb_f and 50 lb_f, respectively. Second, Reynolds number similarity to the previous 2-D testing dictated a Reynolds number approaching 10^6. Third, Wood (14:4) recommends a wing chord/tunnel height ratio of 0.25 or less to minimize tunnel interference effects. With these considerations, simple iteration produced a 20-in. span, 10-in. chord rectangular model. The addition of 1-in. elliptical wing tips resulted in a 22-in. span, 10-in. chord model (aspect ratio 2.2). Slot span remained 20-in. Flow fences were installed just inboard of the wingtips to encourage attached flow on the upper surface.

In addition to force data, pressure data were desired. A total of forty-six pressure taps were distributed at the 1/4 span, 1/2 span and 3/4 span locations (Table I). Surface pressures were monitored to ascertain spanwise flow uniformity and Coanda turning effectiveness.

7
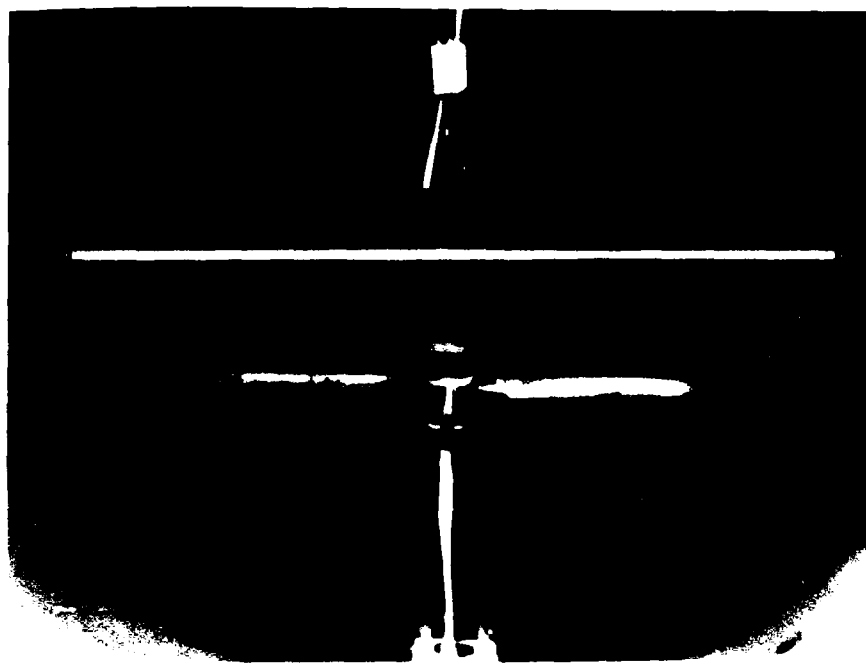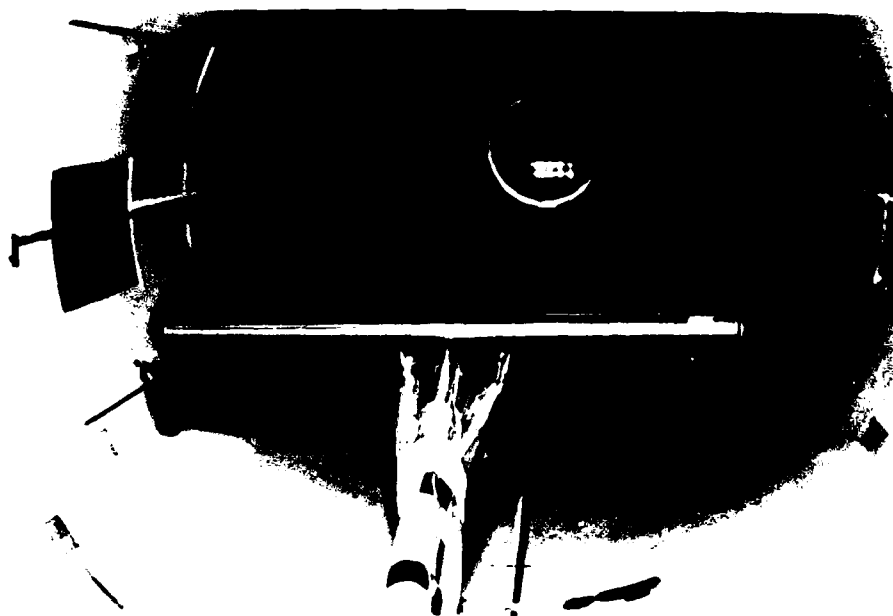
Upstream View

Downstream View

Figure 2. Model Mounted in AFIT 5-ft Wind Tunnel

z ↑
└─→ X
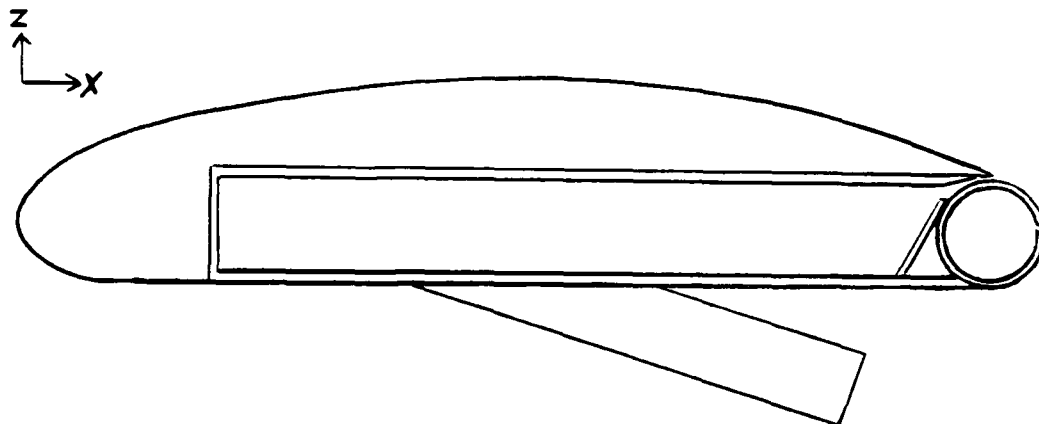
Upper surface:

$$z = 0.27 \left[5^2 - (5 - x)^2 \right]^{1/2} \qquad \text{For} \quad 0 \leq x \leq 9.54\text{-in.}$$

Lower Surface:

$$z = -0.56 \left[1 - (1 - x)^2 \right]^{1/2} \qquad \text{For } 0 \leq x \leq 1\text{-in.}$$

$$z = -0.56 \qquad \text{For } 1 \leq z \leq 9.44\text{-in.}$$

Cylindrical Surface:

$$z = \left[0.56^2 - (x - 9.44)^2 \right]^{1/2} \qquad \text{For } 9.44 \leq x \leq 10\text{-in.}$$

Figure 3. Airfoil Section Geometry

Table I

Surface Pressure Tap Locations

	1/4 Span x/c		1/2 Span x/c	3/4 Span x/c
Upper:	0		0	0
	0.05		0.05	0.05
	0.20*		0.20	0.20
	0.50		0.50	0.50
	0.80		0.80	0.80
Lower:	0		0	0
	0.05		0.05	0.05
	0.20		0.20	0.20
	0.50*		[Sting	0.50
	0.80		Entrance]	0.80
Cylindrical Surface:	0.954	(θ=10 deg)	0.954	0.954
	0.972	(θ=30 deg)	0.972	0.972
	0.993	(θ=60 deg)	0.993	0.993
	1.0	(θ=90 deg)	1.0	1.0
	0.993	(θ=120 deg)	0.993**	0.993
	0.972	(θ=150 deg)	0.972**	0.972
	0.944	(θ=180 deg)	0.944**	0.944

* Plugged
** Rendered inoperable during final assembly

The trailing edge and blowing slots (Figure 4) were designed according to previous work by Englar (15:3). Englar found that strongly attached Coanda jet flow was best maintained for $0.01 \leq h/r \leq 0.05$, where h is the slot height and r is the trailing-edge radius. A trailing-edge radius of 0.56-in. was required to allow the trailing edge to mate tangentially with the chosen airfoil geometry. With r = 0.56-in., both slot heights were designed for 0.02-in, yielding $h/r = 0.036$. To avoid jet flow disturbance, the original slot design did not include slot adjustment screws or slot pins. However, because spanwise slot height uniformity was difficult to maintain, both slots were eventually pinned open in six spanwise locations to maintain the desired height. The location of the primary slot was fixed at 95.4 percent chord. Also, Harvell's 2-D tests indicated favorable results with the secondary slot located between 70 and 80 deg from the primary slot. Thus, 75 deg (99.8 percent chord) was chosen (Figure 4). The small model size did not allow room for hardware needed to make this angle adjustable.

To preserve the integrity of the cylindrical trailing edge, the sting and air hoses entered the wing through the lower surface, making a 16 deg angle with the chord line. With estimated aerodynamic forces based on the test Reynolds numbers, calculations indicated an angle between 10 and 20 deg was required to prevent normal or axial forces from approaching force gauge limits. The original design

11
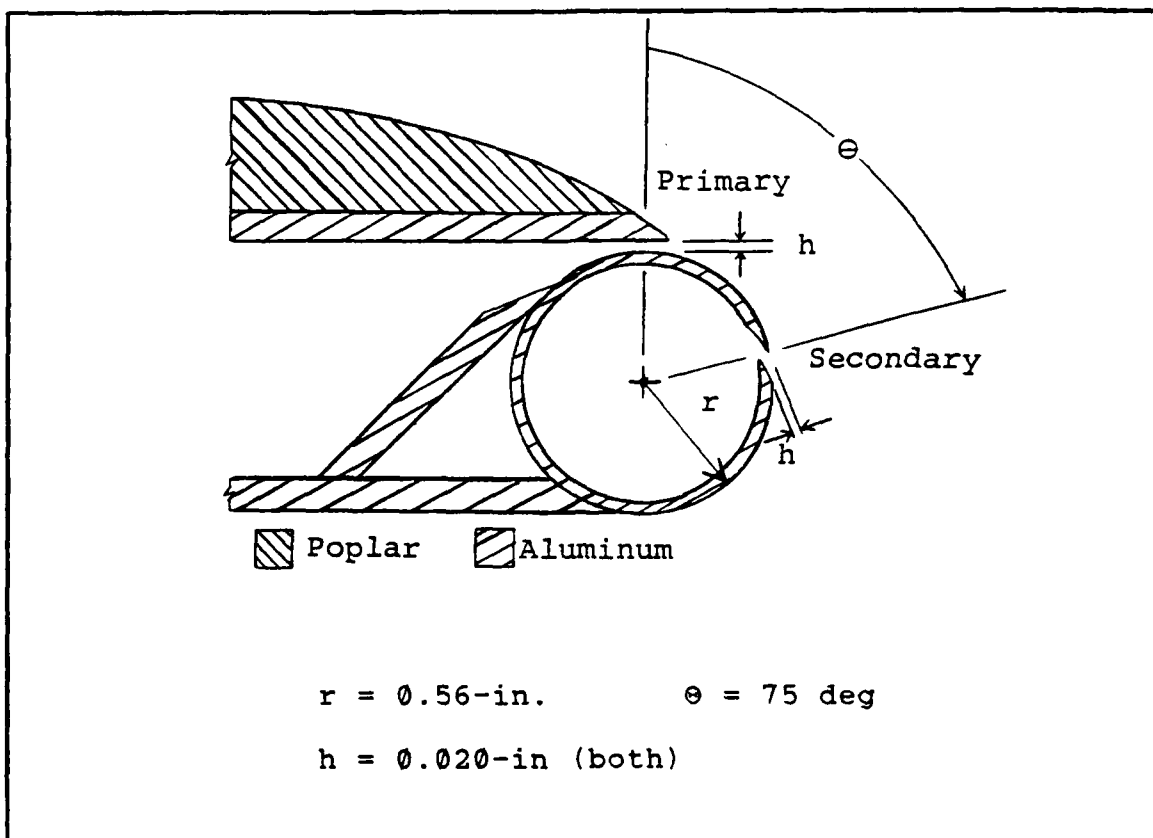
Figure 4. Trailing Edge and Slot Design

stipulated that the two air supply hoses enter the model above and below the sting, to minimize flow/hose interference spanwise. This arrangement required the upper hose to pass through the cylindrical trailing edge and plenum. Again, to preserve the Coanda surface and plenum integrity, this arrangement was abandoned in favor of the side-by-side design pictured in Figure 2.

Internally, the model consisted of two plenum chambers, associated plumbing, and two pressure scanning modules (Figure 5). Each plenum was supplied with air independently. The main plenum, which provided air to the primary slot, was constructed of 1/8-in. aluminum plate.
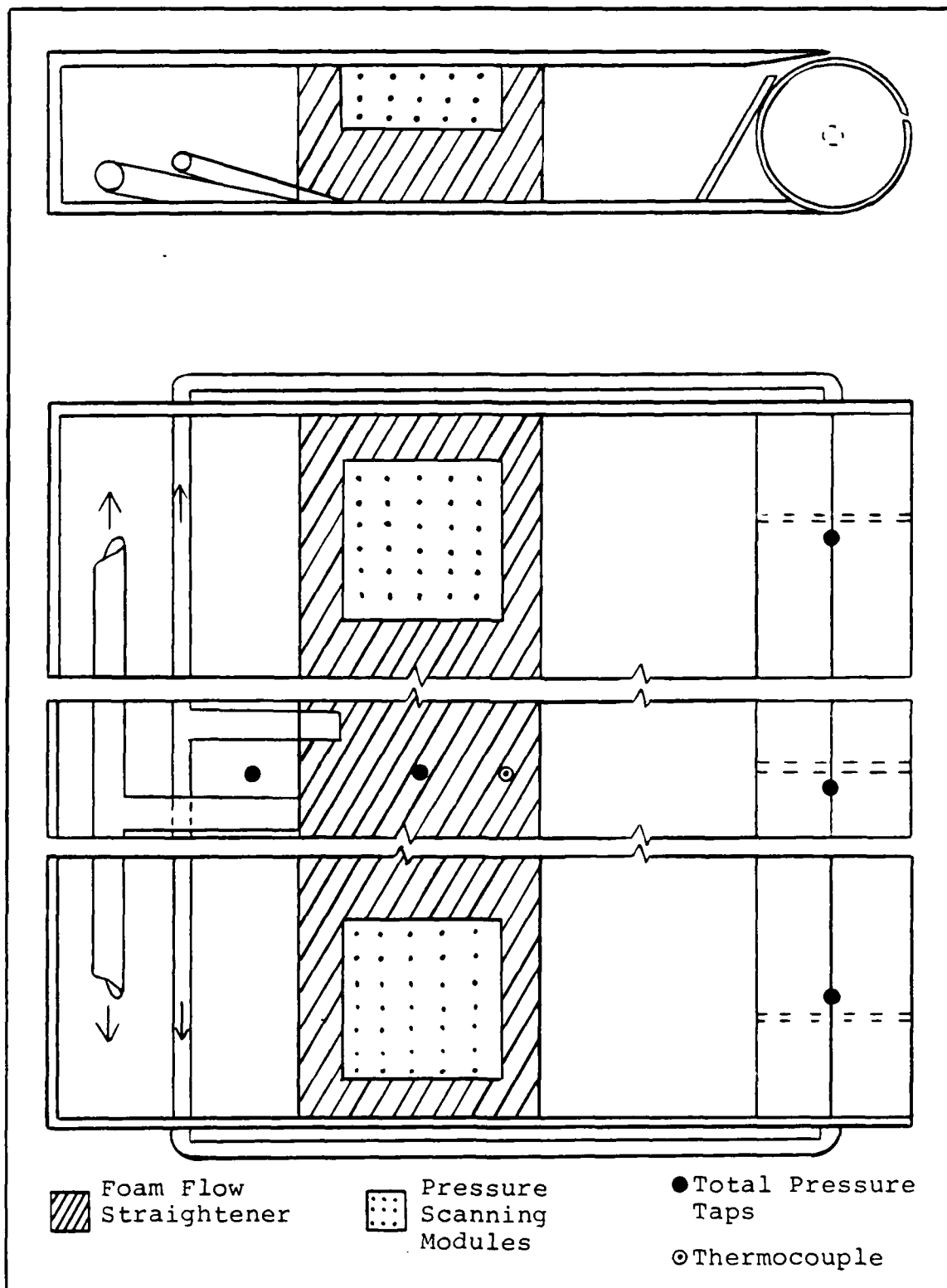
Figure 5. Main and Cylindrical Plenums

13

Foam flow straightener and screens were installed in this plenum to aid in pressure and jet flow uniformity. The main plenum also contained a pressure tap to measure plenum stagnation pressure, and a chromel-alumel thermocouple for temperature monitoring. The cylindrical plenum fulfilled a dual role: it supplied air to the secondary slot, and provided the Coanda surface for both slots. This plenum was constructed of 0.065-in. thick aluminum and was hand finished to ensure uniformity and smoothness. Stagnation pressure taps were also included in this plenum.

Air Supply System

Figure 6 is a schematic of the blowing air supply system. First, the 95 psi field air available in the tunnel facility was routed to a cyclone separator for filtration. Next, the flow passed through a regulator valve, used to vary the plenum pressures. Flow temperature and static pressure were measured via a chromel-alumel thermocouple and pressure gauge, respectively. The supply line split into two distinct lines, each serving one plenum. These lines contained a static pressure gauge, flow valve, and 0.5-in. throat Venturi flow meter. For flow rate measurement, static pressure was measured at each Venturi throat and immediately upstream via flange taps. Fifty-inch U-tube manometers connected to these taps were referenced to atmospheric pressure, producing gauge pressure readings. From these Venturis, the flow reached the model via 1-in. o.d., 3/4-in. i.d. vinyl hoses. The hoses entered the wind
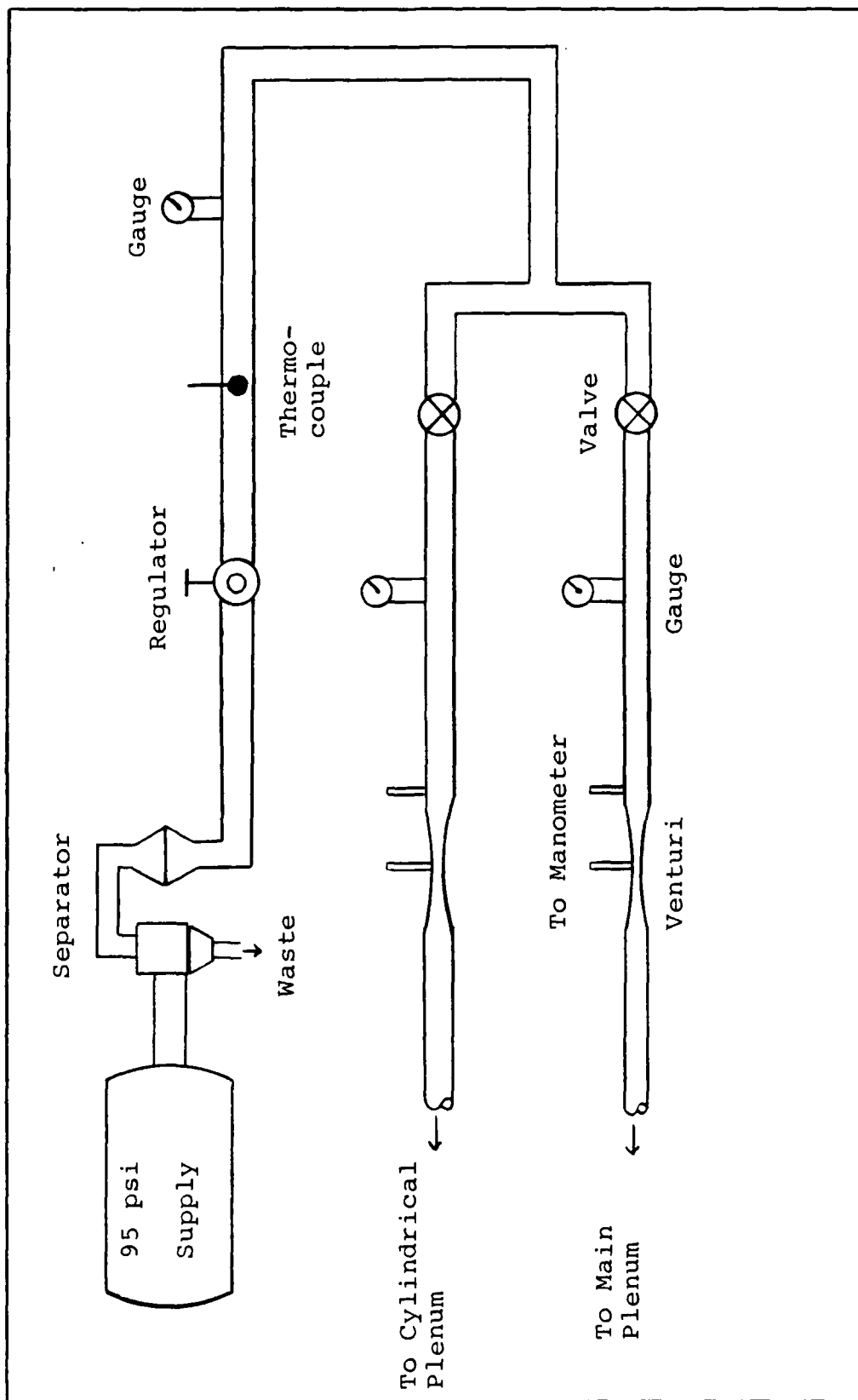
Figure 6. Air Supply System

15

tunnel through two 1-in. circular holes downstream of the test section, and were routed along the sting to the model. Hose sizing was based on a desire to minimize free-stream and jet flow disruption, yet limit pressure head losses. Testing of various hose sizes, along with calculations of expected head losses (Moody chart, Reference 16) resulted in selection of the above sizes.

Wind Tunnel

Wind tunnel tests were performed at the AFIT 5-ft wind tunnel facility at Wright-Patterson AFB. The wooden tunnel was built in 1919 at the old McCook Field in Dayton, OH. It is an open circuit, continuous flow tunnel with a contraction ratio of 3.7 to 1 and a 5-ft diameter closed test section. Flow is induced by two 12 ft counter-rotating fans. Top speed in the test section is 200 mph. Total pressure is atmospheric; static pressure is measured by eight sets of static ports, located 2.5 feet from the tunnel entrance and 11 feet upstream of the test section. A micromanometer displays tunnel dynamic pressure.

The tunnel turbulence factor is 1.5 (17:148) which accounts for the propellers, guide vanes, and tunnel wall vibration. The effective Reynolds number, defined as the product of test Reynolds number (used in this report) and turbulence factor, should be used when comparing test results with flight tests or with data obtained at other tunnel facilities.

Sting Balance/Data Acquisition System

The tunnel is equipped with a 0.5-in. force balance and accompanying data acquisition hardware/software. The 0.5-in Able Corp. Mark V force balance (Figure 7) is a six component strain gauge balance. The six components and their maximum ranges are:

- Two normal force gauges, N1 and N2, for determining normal force and pitching moment (100 lb_f each).
- Two side force gauges, Y1 and Y2, for determining side force and yawing moment (50 lb_f each).
- One axial force gauge, AX (50 lb_f).
- One rolling moment gauge, ℓ (40 in.-lb_f).
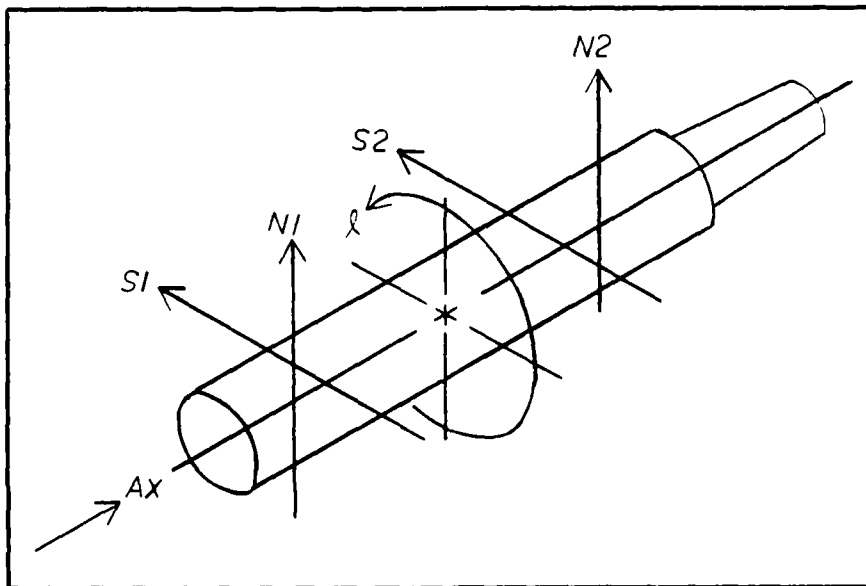
Figure 7.   Six Component Force Balance
(Figure by Able Corp.)

17

Three types of sting balance checks/calibrations were required prior to testing. First, a check loading of the six strain gauges in the force balance was conducted to determine whether the gauge calibration curves were valid. Each gauge was loaded individually in both the positive and negative directions with a series of weights, hung from a calibration body mounted on the balance. Data acquisition and reduction routines (described later) recorded the voltage output from each gauge, and applied existing volts-to-forces calibration curves to convert the voltage outputs into forces. These measured forces were then compared to the known applied loads. Differences in measured and applied loads were less than 2 percent in all instances; this was deemed acceptable. Gauge interactions were negligible. This procedure was repeated, and similar results obtained, near the end of testing. The second type of required calibration was sting angle due to bend. This angle-to-volts curve was automatically generated by the same software routine used to create the existing volts-to-forces curves described above. This calibration curve was used during the reduction of test data to compensate angle measurements for sting bending due to weight. Third, an angle of attack calibration was needed. The model was mounted on the sting and placed at known angles of attack (measured by an inclinometer). Voltage output from the angle of attack potentiometer was recorded and stored.

Calibration software reduced this data into a volts-per-angle curve to be used in test data reduction.

The sting mount has a motorized range of -6 to +26 deg angle of attack and ±6 deg sideslip. In addition, angle of attack "pre-bend" of ±15 deg in 5 deg increments is available, giving the apparatus a total range of -21 to +41 deg angle of attack.

A digital data acquisition/reduction system works in conjunction with the force balance. The system hardware includes a Hewlett-Packard 3852A Data Acquisition/Control Unit (DACU), an IEEE-488 interface bus, and a Zenith Z-248 computer (Figure 8). The user is afforded complete control of all aspects of the system through the Zenith Z-248 and system software. The system software library consists of routines for all force balance calibrations and force/moment data collection, reduction and presentation. The data reduction routines allow force and moment data to be presented in aerodynamic coefficient form, referenced to either wind, stability, or body axes systems (for a discussion of these axes systems, see Roskam (18)). Other data collected by the system through the DACU include tunnel static pressure and free-stream temperature. Atmospheric pressure (tunnel total pressure) is a manual entry, used with tunnel static pressure to calculate tunnel dynamic pressure with the familiar Bernoulli equation. Reference 19 gives a description of these routines with instructions on their use.
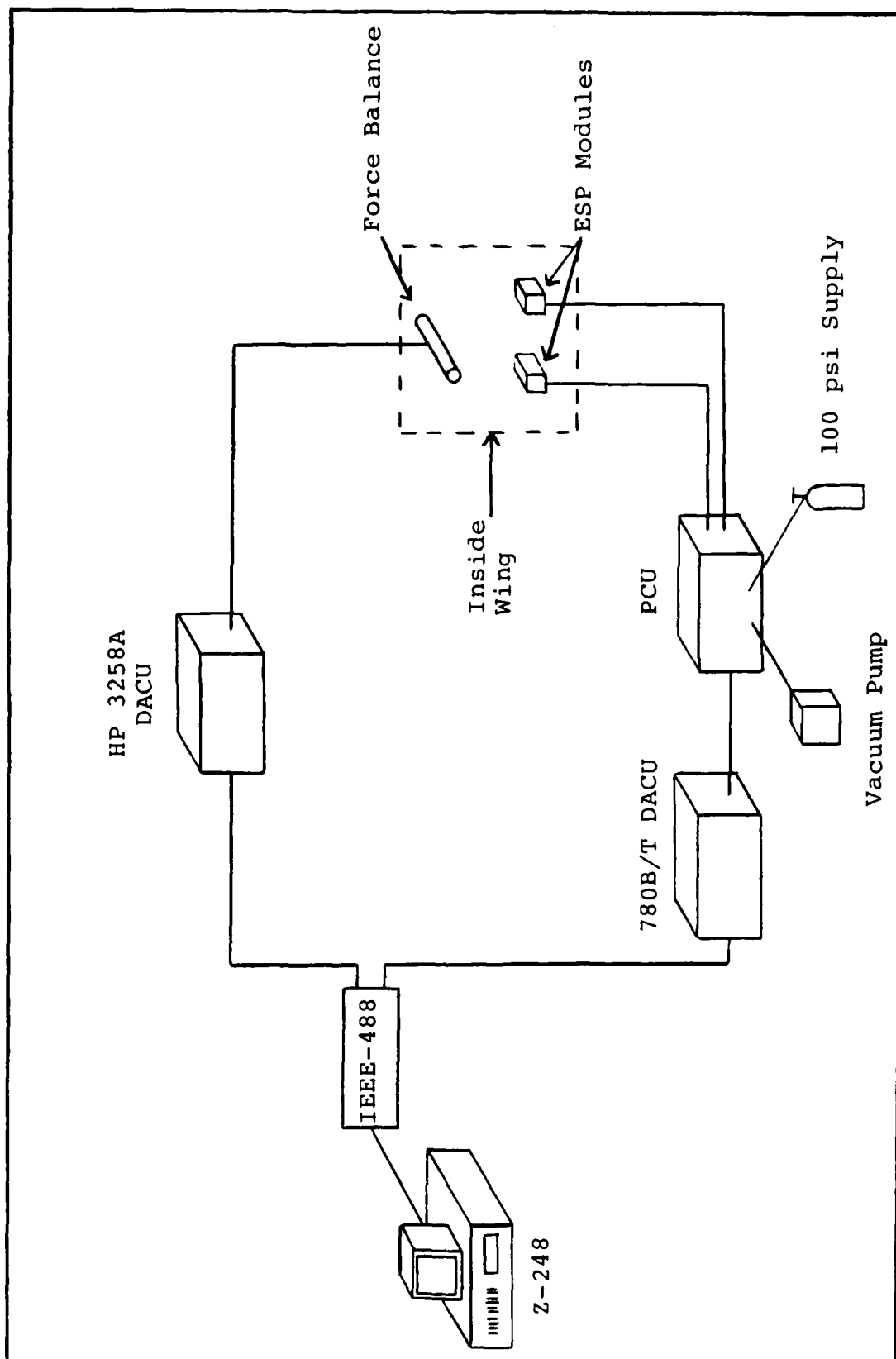
Figure 8. Data Acquisition System

Pressure Measurement System

A 780B/T Pressure Measurement System (Pressure Systems, Inc., Reference 20) was used to collect model surface pressures and plenum pressures. This system is an electronic pressure measuring system designed for multi-pressure measurement applications. Data scan rates of up to 20,000 measurements per second are possible. The major components include the system controller (the Zenith Z-248 computer mentioned previously), the IEEE-488 interface bus, the data acquisition and control unit (DACU), the pressure calibration unit (PCU), and electronically scanning pressure (ESP) modules (Figure 8). The Z-248, with the system software, provides complete control over all data acquisition/reduction and system calibration. The PCU consists of three pressure regulators and three quartz pressure transducers used to calibrate the ESP modules. The ESP modules are pressure sensors consisting of 32 ports, with each port possessing its own pressure-to-volts transducer. These ports measure a pressure differential (pounds per square inch differential, or psid) in local pressure from a known reference pressure, typically atmospheric. Model pressure taps are connected to these ports with conventional pressure tap tubing. Two ESP modules were encased inside the wing model to measure surface and plenum pressures.

Typical system operation combines data collection with the on-line calibration capability. Upon commands from the

21

controller (through the DACU), the PCU directs 100 psi air to a calibrate/operate valve in the ESP modules, tripping the valve to the calibrate position. Next, the PCU sends three pre-set calibration pressures to each ESP module port. The ports measure the calibrate pressure/reference pressure differentials and send voltages to the DACU. For each port, the DACU generates a volts-to-pressure curve of the form:

$$P = C0 + C1(V) + C2(V^2) \qquad (2)$$

The coefficients C0, C1, and C2 for each transducer are stored and used to calculate pressures during testing.

For this test, the system software was integrated with the force data acquisition software, allowing concurrent force data/pressure data collection.

III. Experimental Procedure

Checkouts

With a dual-slot arrangement, secondary-slot blowing is beneficial only if primary-slot blowing is accomplished successfully. Accordingly, initial emphasis was placed on establishing quality primary-slot blowing. Due to disappointing primary-slot performance and limited wind tunnel access, secondary-slot blowing was not accomplished. Total emphasis was eventually placed on improving wing performance with primary-slot blowing only.

Prior to active wind tunnel testing, several checkout procedures were accomplished. First, as the main plenum was slowly pressurized over its operational range, the model was checked for leaks. Although one leak was detected near the leading edge, it was very small and considered negligible. Next, a primary-slot jet velocity survey was conducted to investigate the spanwise uniformity of the jet. The main plenum was pressurized, and a total-head probe, connected to a micromanometer and mounted on a traverse, was inserted into the jet exit plane. Total head was measured every 1/2-in along the slot, and results converted to velocity. Also, with the plenum still pressurized, slot height was measured to investigate spanwise variation. Last, the on-board pressure transducers were electronically calibrated, and all pressure ports were checked for blockage, leakage, and correct tube designation.

23

Finally, model weight tares were accomplished with the force balance data acquisition system. These tares provided the model weight and CG location (referenced to balance center), which were stored and used during test data reduction. During actual testing, the data reduction routines subtract model weight from measured forces. With the wind tunnel off and the model mounted on the sting at zero roll and zero sideslip angles, force data was collected at a series of pitch angles. Tare reduction routines in the system software library solved a set of equations with a least squares regression technique to find 1) the effect of model weight on each strain gauge, and 2) the moment arms from model CG to balance CG along each balance axis.

Preliminary Testing

Tare runs were needed to determine the aerodynamic effect of the air supply hoses on the strain gauge balance. The tunnel was run and force data collected on a clean model (no air hoses attached) at angles of attack of -6 to 6 deg. Next, the air hoses were attached, but no blowing air used; force data was again collected throughout the same angles and tunnel speed. All force data was converted to aerodynamic coefficients and plotted (Figures 9, 10, and 11). The difference in these two data sets was the aerodynamic effect of the air supply hoses and was used as a correction to later test results. Although these tests were run at both test Reynolds numbers, the data indicated no Reynolds number dependence.
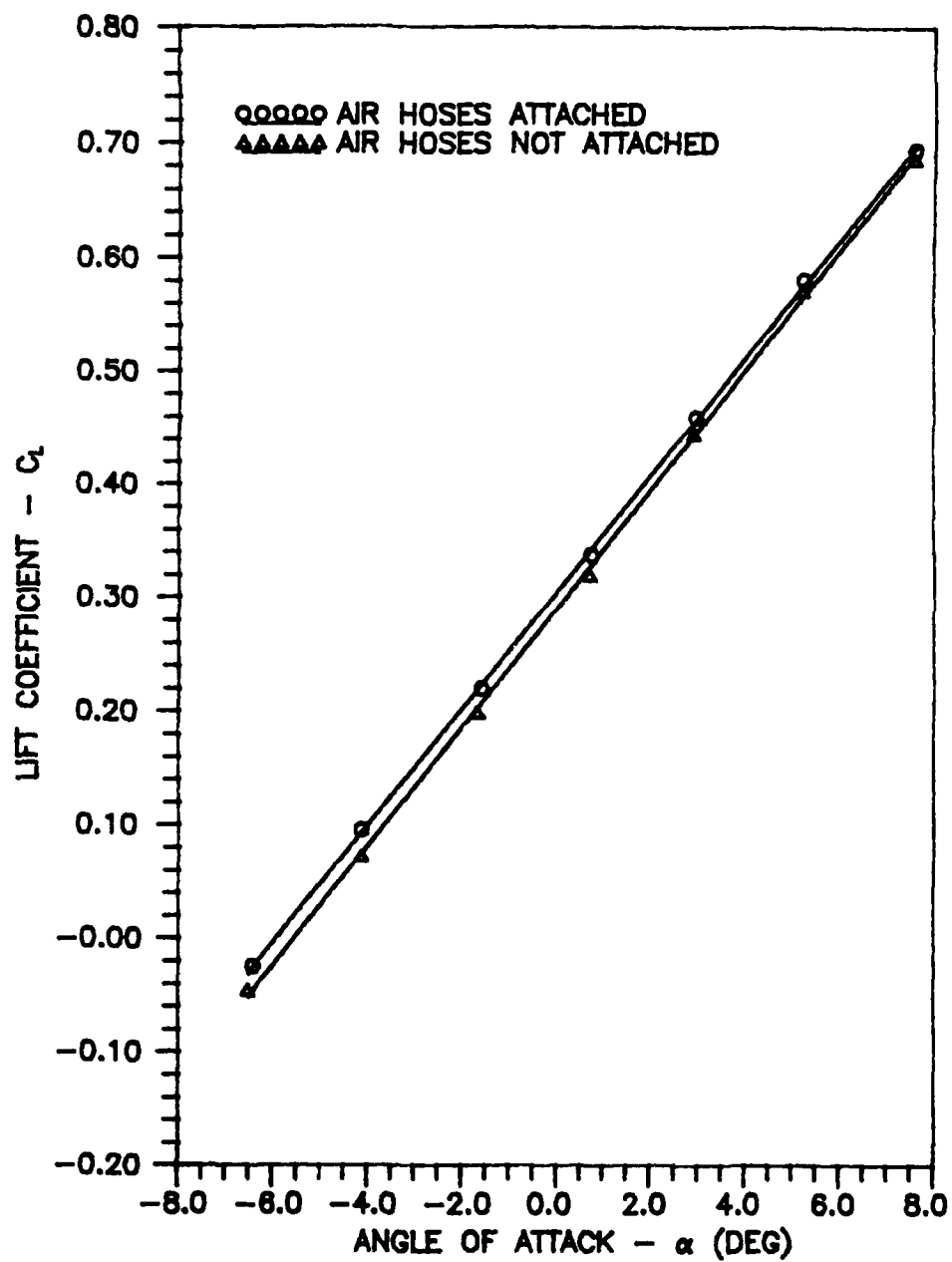
Figure 9.   Lift Coefficient vs. Angle of
            Attack, $C\mu=0$

25
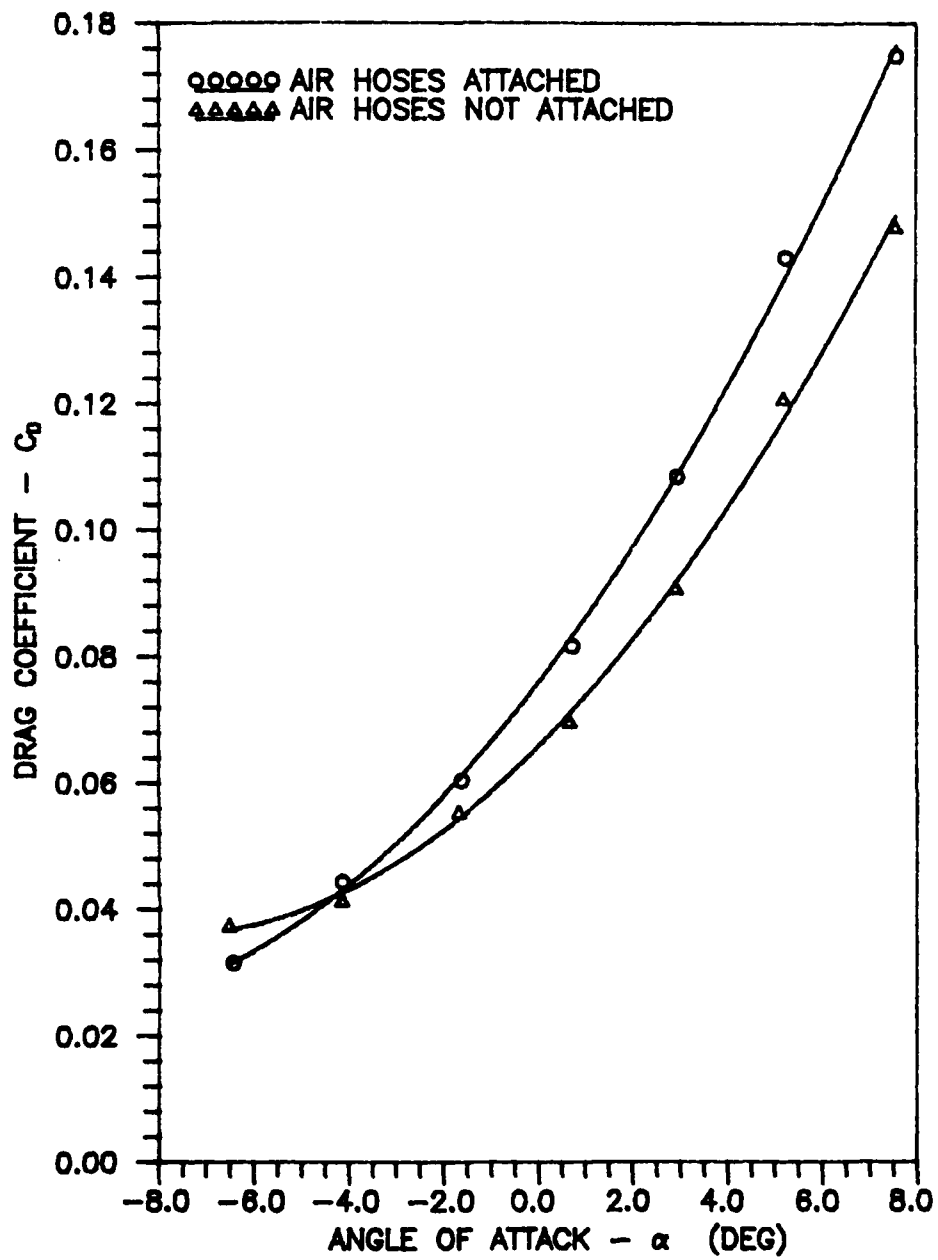
Figure 10. Drag Coefficient vs. Angle of
Attack, $C\mu=0$

26
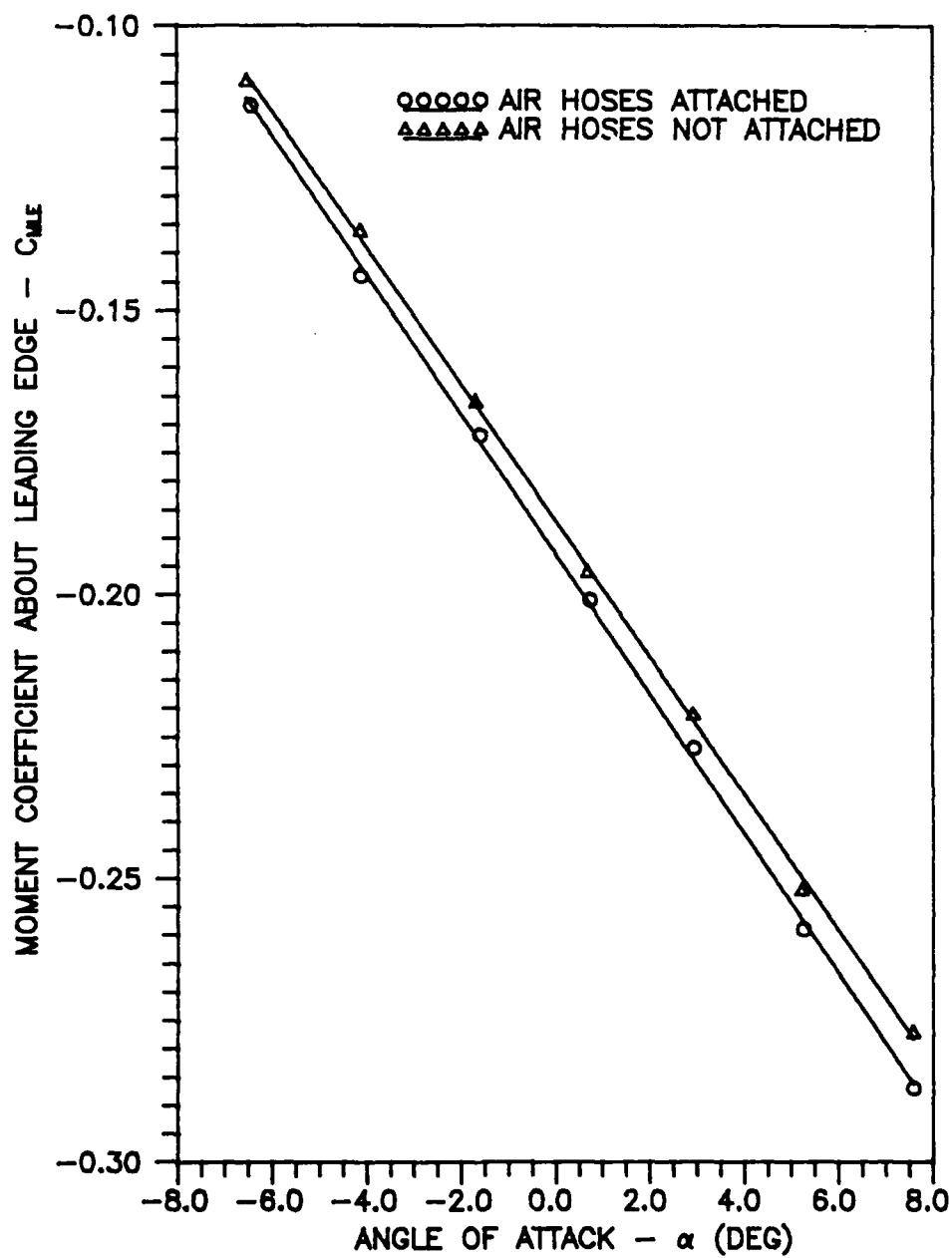
Figure 11.   Pitching Moment Coefficient vs. Angle of
Attack, Cμ=0

Tare runs were also needed to determine the effect of the blowing air on the balance. With the wind tunnel off, primary-slot blowing was accomplished over the entire range of main plenum pressures. Normal and axial force data was collected, plotted versus jet mass flow rate, and used as a correction to later test results (Figure 12).

Finally, since the air supply tubes were strapped to the sting and entered the model without bending, no "Bourdon tube" forces (due to a tube's tendency to straighten under pressure) existed.

Primary Testing

$Re = 9x10^5$. Testing was accomplished at angles of attack from -6 to 6 deg in 2 deg increments. At each angle of attack, primary-slot blowing was varied from zero to the maximum available. Blowing was controlled by setting an upstream Venturi pressure. At each point, the data acquisition systems (both force balance and pressure) collected force data, free-stream data (temperature, pressures), and model pressures (surface and plenum). Atmospheric pressure, ambient temperature, Venturi pressures, blowing air temperature, and plenum stagnation temperature were recorded manually. Repeatability was verified throughout as redundant runs were made. The model was then fitted with nylon tufts, and flow visualization runs were accomplished throughout the angle of attack and blowing ranges.
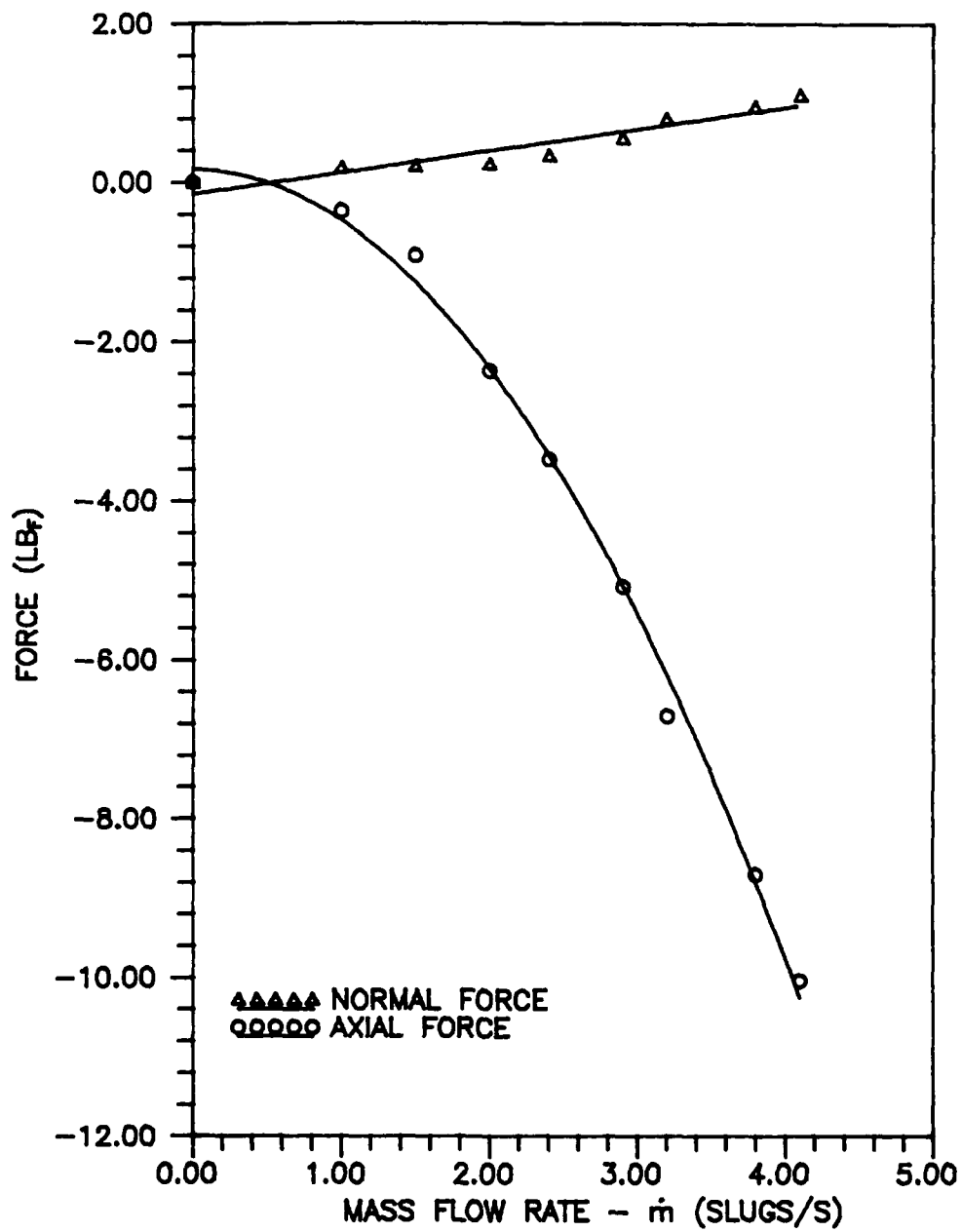
Figure 12. Primary-Jet Reaction on Normal and Axial Force Elements

$\underline{Re = 6x10^5}$. Based on test results obtained at $Re = 9x10^5$, testing at $Re = 6x10^5$ was deemed necessary. Testing was accomplished at angles of attack from -4 to 4 deg in 2 deg increments. Overall procedures were identical to those described above. Again, flow visualization runs were conducted over the entire angle of attack and blowing ranges.

IV. Data Reduction

The reduced data required for analysis included the
following: momentum coefficient (Cμ), lift coefficient
(C_L), drag coefficient (C_D), equivalent drag coefficient
(C_{DE}), pitching moment about the leading edge (C_{Mle}),
lift-to-equivalent drag ratio (L/D_E), and pressure
coefficient (C_p). The data reduction software utilized with
the sting balance reduced the measured loads into C_L and C_D
coefficients. An external, Basic routine was written to
calculate C_{Mle} from force data; C_{DE}, L/D_E, and C_p were
computed manually.

Momentum Coefficient

The blowing parameter used as the independent variable
in circulation control studies is the momentum coefficient,
defined as the momentum of jet air issued from the slot,
nondimensionalized:

$$C\mu = \frac{\dot{m}_j v_j}{q_\infty S} \tag{3}$$

The jet mass flow rate, $\dot{m}_j$, was obtained by measuring the
static pressure at the Venturi throat, and static pressure
and temperature upstream of the Venturi. Assuming
isentropic flow, and combining the first law of
thermodynamics with continuity, one obtains:

$$\dot{m}_j = C_d A_2 \frac{[2P_1(P_1 - P_2)]^{1/2}}{[RT_1\{1 - (A_2/A_1^2)\}]^{1/2}} Y \tag{4}$$

31

where Y is a compressibility factor, C_d is the coefficient of discharge for the Venturi, and subscripts 1 and 2 signify conditions upstream and at the Venturi throat, respectively. The compressibility factor Y is a rather complicated function of Venturi A_2/A_1 and P_2/P_1; its use simply allows the above equation to be written in a form similar to its incompressible form. Working plots of Y for a range of pressure and area ratios can be found in some fluid mechanics texts. The jet velocity in the slot exit plane, v_j, was calculated by assuming isentropic expansion from plenum stagnation pressure. Using the isentropic relation

$$P_t/P_j = [1+(k-1)M_j^2/2]^{k/(k-1)} \tag{5}$$

and substituting in both the definition of Mach number

$$M_j^2 = v_j^2/(kRT_j) \tag{6}$$

and the isentropic relation

$$T_t/T_j = 1+(k-1)M_j^2/2 \tag{7}$$

one obtains (upon rearrangement)

$$v_j = \left[\frac{2kR}{(k-1)} T_t \left\{ 1 - (P_j/P_t)^{\frac{k-1}{k}} \right\} \right]^{1/2} . \tag{8}$$

This development of v_j requires isentropic jet expansion from plenum stagnation pressure to static pressure in the slot exit plane. However, to reduce model geometry and orientation effects, v_j is generally calculated using

expansion to free-stream static pressure. For ease of
comparison with other circulation control test data, the
latter method was used.

Lift Coefficient

Figure 13 shows the orientation of the two normal
force elements (N1, N2) and axial force element (AX) of the
sting balance. The measured lift coefficient is defined as:

$$C_L = \frac{(N1+N2)\ \cos(\alpha+16)\ -\ AX\ \sin(\alpha+16)}{q_\infty S} \qquad (9)$$

where $(\alpha+16)$ can be thought of as the force balance angle of
attack. This C_L was calculated by the system data reduction
routines. Several corrections to this measured C_L were then
made. First, to reflect lift generated by the wing only,
the lift generated by the air supply hoses was subtracted.
This correction is the difference of the two curves
presented in Figure 9. Also, to present the data as a
function of $C\mu$ for particular angles of attack, slight
adjustments were made to account for sting bending. Using
the "hoses attached" curve of Figure 9, that part of
measured C_L attributable to a slight deviation in angle of
attack was identified and subtracted. Finally, by
convention the jet reaction force acting in the lift
direction should be subtracted from the measured lift. In
this way, only lift due to circulation is presented,
facilitating comparison with circulation control airfoil
data. Accordingly, C_L attributable to the jet reaction

33
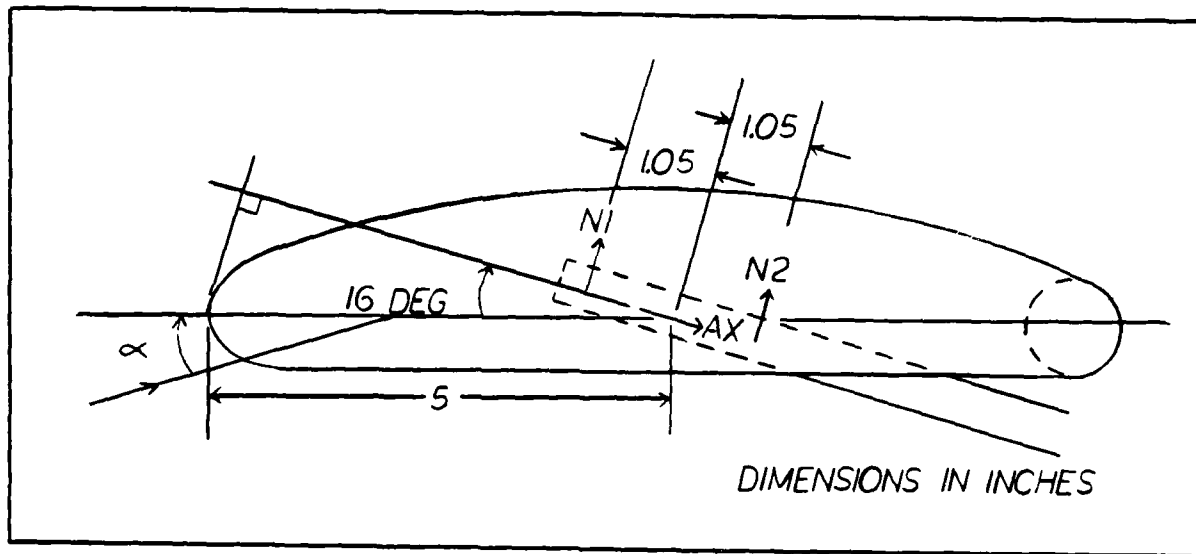
Figure 13. Wing/Force Balance Orientation

force was calculated from the force data of Figure 12 and subtracted from measured C_L. Although all corrections were quite small compared to measured C_L, they were included for completeness. Table II is a representative example of the magnitudes of these corrections.

Drag Coefficient

From Figure 13, the measured drag coefficient is defined as:

$$C_D = \frac{(N1+N2)\ \sin(\alpha+16)\ +\ AX\ \cos(\alpha+16)}{q_\infty S} \qquad (10)$$

This measured C_D was calculated by the system data reduction routines. The same type of corrections made to C_L for air

34

Table II

Representative Data Corrections

$\alpha = 0$, $Re = 9 \times 10^5$

Lift

$C\mu$	measured C_L	hoses	sting bend	thrust	C_L
0	0.317	-0.015	-0.02	0	0.282
0.004	0.333	-0.015	-0.02	-0.004	0.294
0.009	0.353	-0.015	-0.02	-0.010	0.308
0.016	0.398	-0.015	-0.02	-0.019	0.344
0.023	0.419	-0.015	-0.02	-0.028	0.356
0.032	0.472	-0.015	-0.02	-0.041	0.396
0.041	0.519	-0.015	-0.02	-0.053	0.431
0.053	0.549	-0.015	-0.02	-0.069	0.445
0.061	0.583	-0.015	-0.02	-0.080	0.468

Drag

$C\mu$	measured C_D	hoses	sting bend	thrust	C_D
0	0.081	-0.01	-0.006	--	0.065
0.004	0.072	-0.01	-0.006	--	0.056
0.009	0.067	-0.01	-0.006	--	0.051
0.016	0.051	-0.01	-0.006	--	0.035
0.023	0.036	-0.01	-0.006	--	0.020
0.032	-0.005	-0.01	-0.006	--	0.021
0.041	-0.046	-0.01	-0.006	--	0.062
0.053	-0.085	-0.01	-0.006	--	0.101
0.061	-0.114	-0.01	-0.006	--	0.130

Pitching Moment

$C\mu$	measured C_{Mle}	hoses	sting bend	thrust	C_{Mle}
0	-0.197	+0.005	+0.005	--	0.187
0.004	-0.206	+0.005	+0.005	--	0.196
0.009	-0.219	+0.005	+0.005	--	0.209
0.016	-0.243	+0.005	+0.005	--	0.233
0.023	-0.255	+0.005	+0.005	--	0.245
0.032	-0.283	+0.005	+0.005	--	0.273
0.041	-0.307	+0.005	+0.005	--	0.297
0.053	-0.320	+0.005	+0.005	--	0.310
0.063	-0.338	+0.005	+0.005	--	0.328

hose effects and sting bending were applied to C_D, this time using the curves of Figure 10.

Equivalent Drag

The measured drag can and will be negative at times, due to the thrust reaction of the jet. To allow direct comparison of efficiency with unblown wings, and to avoid unrealistic infinite efficiencies when measured drag is zero, an equivalent drag was used and defined as (20:11, 21:15):

$$D_E = D + \text{jet reaction} + \frac{\dot{m}_j v_j^2}{2 v_\infty} + \dot{m}_j v_\infty \qquad (11)$$

This equivalent drag term takes into account the energy expenditures required to produce the blowing. The first and second terms on the right side are the measured drag and jet thrust effect, respectively. The third term represents the power expended in compressing air from free-stream static pressure to plenum stagnation pressure, while the last term is a ram inlet penalty. Nondimensionalizing by dynamic pressure and reference area produced the equivalent drag coefficient, C_{DE}.

Pitching Moment about the Leading Edge

Again referring to Figure 13, the pitching moment about the leading edge is defined as:

$$C_{Mle} = \frac{AX[5\sin(16)] - N1[5\cos(16) - 1.05] - N2[5\cos(16) + 1.05]}{q_\infty S c} \qquad (12)$$

Corrections for hose effects and sting bend were accomplished in the previously described manner, using Figure 11. Per convention, jet reaction effects were included in this coefficient.

Pressure Coefficient

Although this research relied on force data in determining aerodynamic coefficients, pressure data was useful in understanding flow field characteristics. Pressure data is presented in the form of a pressure coefficient, defined as:

$$C_p = \frac{P - P_\infty}{q_\infty} \qquad (13)$$

As the electronic pressure measurement system presents pressure readings as a differential from atmospheric, it is more convenient to rewrite this expression as:

$$C_p = \frac{P - P_{atm}}{q_\infty} + 1 \qquad (14)$$

This derivation assumes subsonic flow, with tunnel total pressure equal to atmospheric pressure.

Wind Tunnel Corrections

Sound wind tunnel practice dictates that tunnel-boundary corrections be applied to all test data. These corrections take into account the effect of tunnel walls on the free-stream flow. Pope (17) discusses the theory and use of these corrections in some detail. Four such corrections were applied to the test data: buoyancy, solid blockage, wake blockage, and induced drag. Buoyancy

37

corrections are needed due to a thickening of the wall boundary layer as the flow progresses through the tunnel, causing a negative pressure gradient in the test section. This pressure gradient tends to "draw" the model downstream and predominantly effects drag measurements. Solid blockage effects arise from the model's presence in the test section, effectively reducing the area through which the free-stream may flow. By continuity, this area reduction causes a velocity increase about the model, affecting all test data. Wake blockage effects are similar in nature to solid blockage effects. Since the flow velocity in a model's wake is lower than the free-stream, the flow velocity just outside the wake must be greater than free-stream to satisfy continuity. According to Bernoulli's law, this velocity increase results in a negative pressure gradient, predominantly affecting drag measurements. Finally, the tunnel walls tend to diminish the downwash of a lift-generating wing, reducing induced drag (i.e., the drag due to lift). Corrections for these four effects were applied during data reduction.

A fifth correction (not considered a wall boundary correction) was made for dynamic pressure "skew" (19:18). Prior research found that actual dynamic pressure in the test section differed from measured dynamic pressure by 2 percent, due to the upstream location of the static pressure taps. This correction was also applied by the system data reduction software.

V. Results and Discussion

Preliminary Testing

Test results are for primary-slot blowing only. As described in Section III, the first series of tests involved slot height measurement and jet flow surveys. Results of the jet velocity survey and slot height measurements were disturbing. Figure 14 shows one example of these measurements. The slot height variation was extreme, with a corresponding non-uniform jet velocity profile. To correct the slot height, tear-drop washers were installed just inside the slot exit plane. The washers were installed symmetrically; starting from the left, one each was located at the 1,4.5,8.5,11.5,15.5, and 19-in. locations. The jet flow survey and slot height measurements were again conducted; representative results are plotted in Figure 15. Although not ideal, the slot height variation was vastly improved. Jet flow uniformity was adequate except at mid-span, where the internal plenum flow must negotiate around the sting mounting block protruding into the main plenum.

From the preliminary tare runs described in Section III, the lift, drag, and moment results (Figures 9, 10, and 11) at zero angle of attack were in close agreement with the 2-D airfoil data (accomplished for zero angle of attack only). A tuft study of the primary-slot jet flow (tunnel off) indicated a jet turning of approximately 70 deg, again similar to 2-D results.
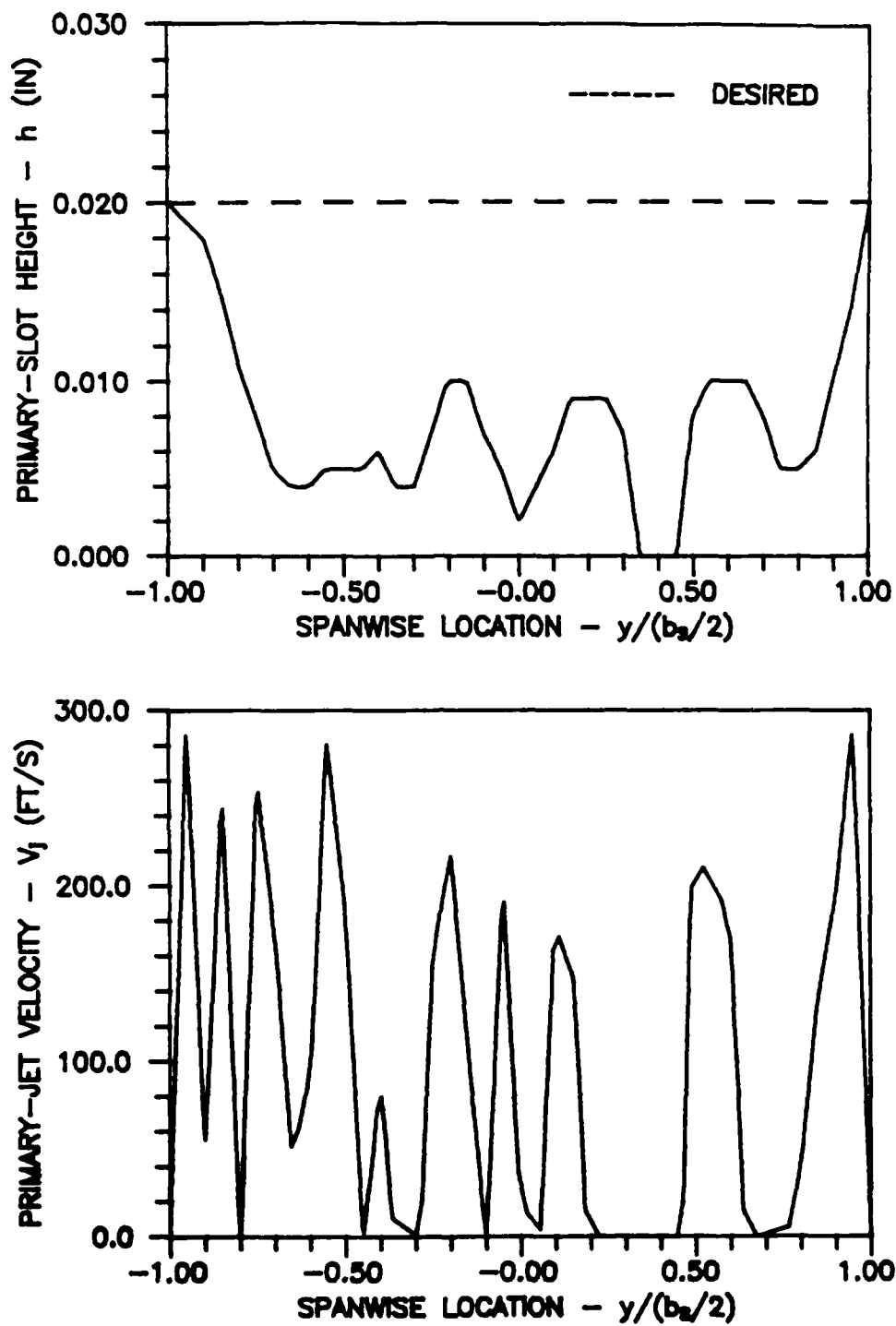
Figure 14. Example of Primary-Slot Height and Jet Velocity Before Slot Modification, $\dot{m} = 6.5 \times 10^{-4}$ slugs/s
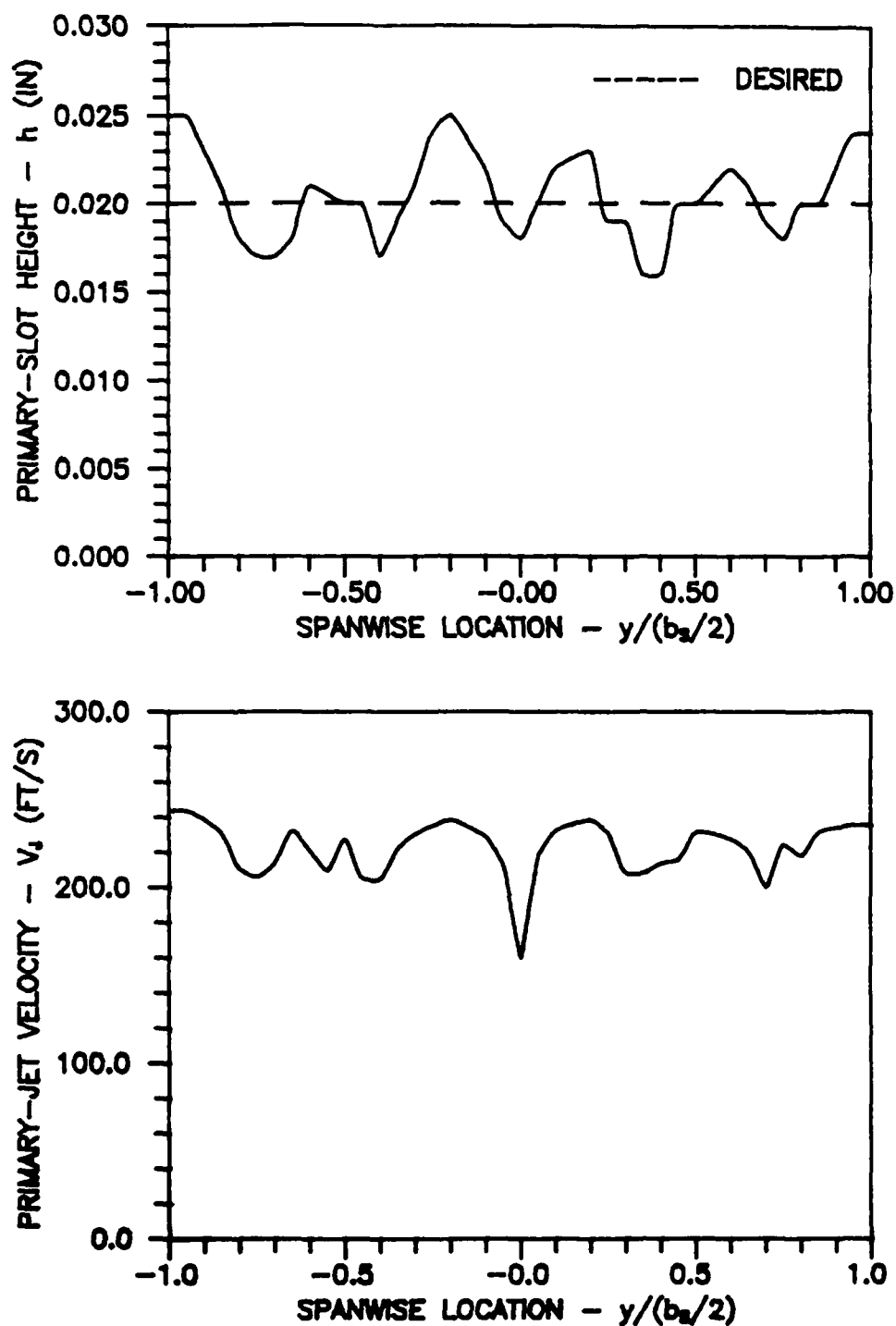
Figure 15. Example of Primary-Slot Height and Jet Velocity After Slot Modification, $\dot{m} = 1.3 \times 10^{-3}$ slugs/s

Primary Testing

$\underline{Re = 9x10^5}$. Lift results as a function of momentum coefficient and angle of attack are presented in Figure 16. These curves display a gradual increase in lift coefficient as blowing is increased. The rate of lift augmentation, $dC_L/dC\mu$, is fairly constant with very little dependence on angle of attack. Based on a comparison with previous 2-D test results obtained with this section, this lift augmentation rate is somewhat less than anticipated, being approximately 15 percent of the equivalent 2-D lift augmentation rate. A 2-D vs. 3-D comparison must be made rather loosely, however, keeping in mind the low wing aspect ratio of 2.2. Aerodynamic performance of low aspect ratio wings customarily falls well short of airfoil performance (22:176).

Further insight into the effects of the blowing jet is provided by the experimental pressure distributions of Figures 17 through 19. First, note that the number of pressure taps at any one spanwise location was not sufficient to produce a pressure distribution curve of great accuracy. The original intent of these taps was to determine spanwise flow uniformity only, which was found excellent for all test conditions. However, some insight into conditions at the trailing edge can be gained through these plots. Figures 17 through 19 represent conditions at either the 1/4 or 3/4 span locations (they were identical) for zero angle of attack and momentum coefficients of 0,

42

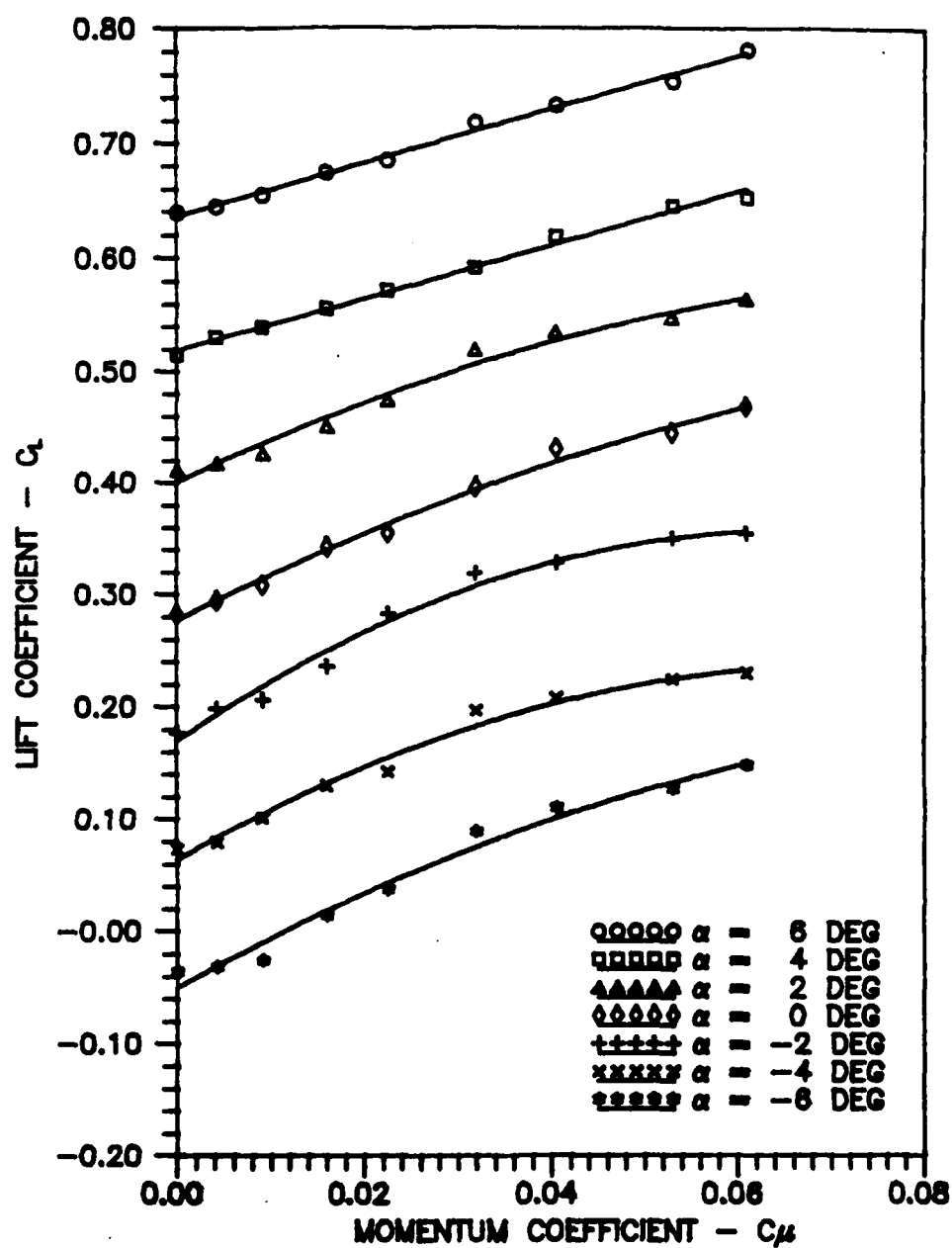Figure 16. Lift as a Function of Momentum Coefficient,
Re=9x10^{5}

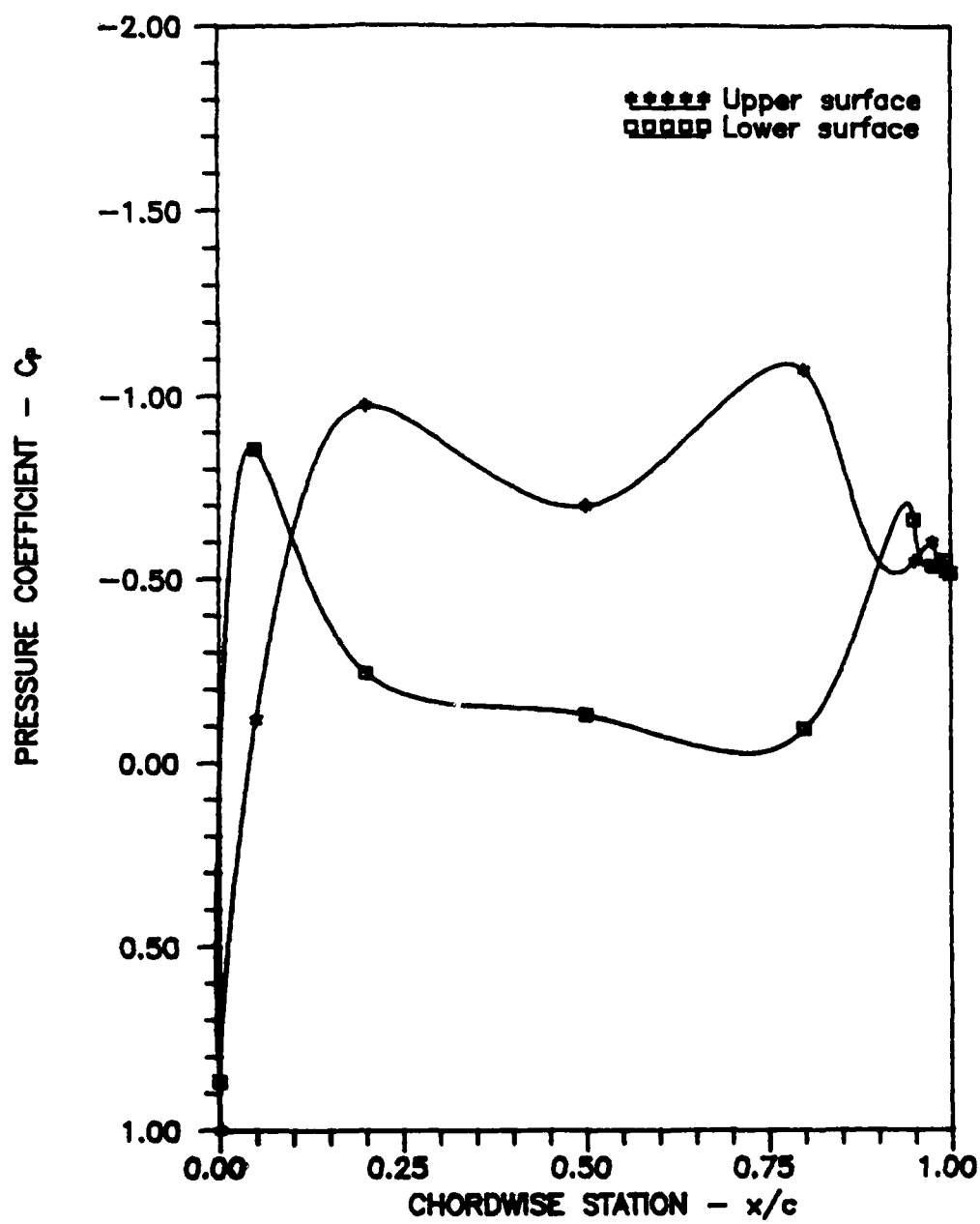Figure 17. Pressure Distribution at Cμ=0, α=0, Re=9x10^{5}

44
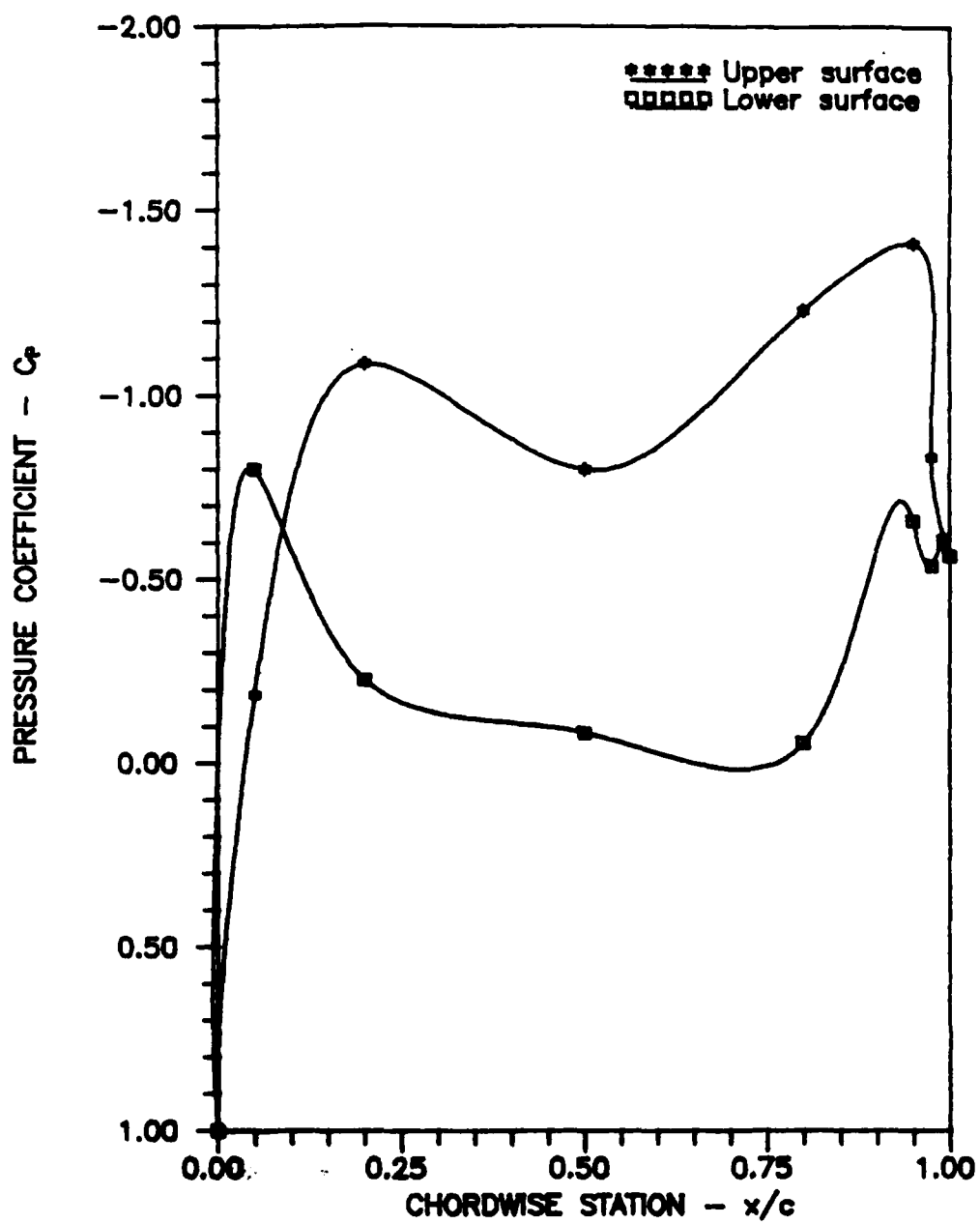
Figure 18. Pressure Distribution at Cμ=0.032, α=0,
Re=9x10^{5}
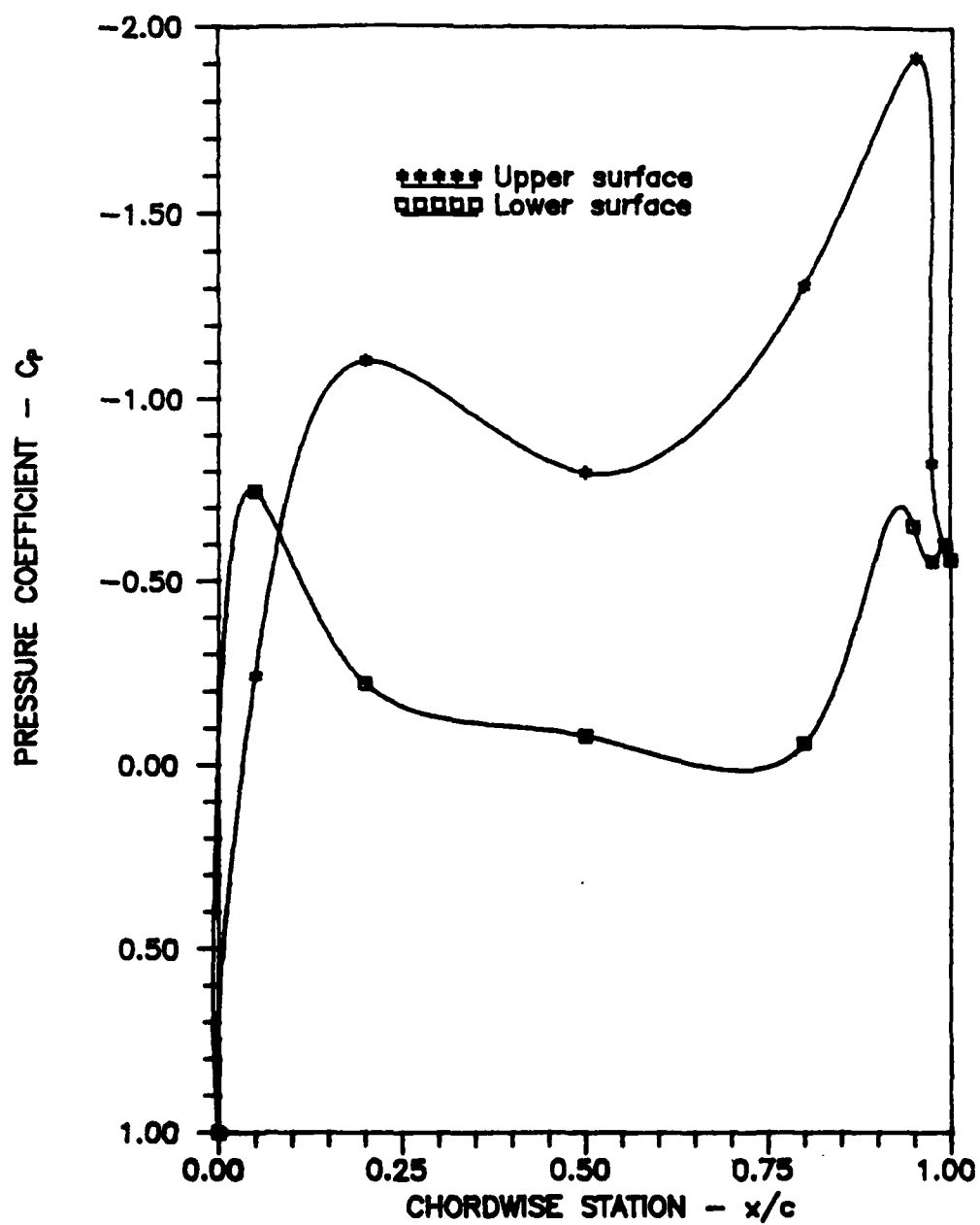
Figure 19. Pressure Distribution at Cμ=0.053, α=0, Re=9x10^5

46

0.032, and 0.053. Each of these figures shows a rather steep positive increase in pressure coefficient as the flow reached the cylindrical aft surface (x/c = 0.95), indicating a severe, adverse pressure gradient and the onset of separation. For the jet off case (Figure 17), this increase began well upstream, near x/c = 0.75. Also, the peak on the lower surface near x/c = 0.90 indicates that an adverse pressure gradient was later to develop on the lower surface. As blowing was increased (Figures 18-19), a suction peak just downstream of the slot exit became pronounced, extending the region of attached flow beyond the slot--but the peak was short lived. The sharp increase in pressure coefficient occurred just aft of the slot, indicating that strong Coanda turning around the cylindrical surface was not present. Strong jet turning would be evidenced by much smaller pressure coefficients in the trailing-edge region. Integrating these pressure distributions with cubic-spline quadrature produced 2-D lift coefficients in close agreement with measured lift coefficients.

Generally, elliptical sections can have difficulty sustaining attached flow, even at low angles of attack. However, From previous testing (conducted at the same Reynolds number), this elliptical upper surface design was able to sustain attached flow beyond x/c = 0.95. Also, the trailing-edge pressure characteristics (Figures 17-19) show little angle of attack dependence for $-6 \leq \alpha \leq 6$ deg. These

47

two details suggest the upper surface geometry was not a cause for early separation.

Referring to Figure 4, the jet exited the slot parallel to the chord line at the uppermost point of the trailing-edge cylinder. This trailing edge and slot design appeared capable of Coanda turning during the tuft studies previously mentioned. However, this configuration required the jet to attach to the cylinder wall, and begin turning, immediately upon exiting the slot. A freestream-induced adverse pressure gradient on the cylindrical surface would render initial jet attachment difficult, especially at positive angles of attack. A slight aft movement of the trailing-edge cylinder, requiring the jet to attach to the cylindrical surface just before turning, may be appropriate. Also, a slight undercut in the slot upper wall to initially deflect the jet down onto the cylinder may be beneficial.

Drag results are plotted in Figure 20 as a function of momentum coefficient and angle of attack. As expected, the drag in the unblown case was fairly high, due to the large momentum losses behind the bluff trailing edge. Also typical of circulation control wings was the drag decrease with increased blowing, eventually resulting in negative drag. This is due partially to jet entrainment of the local flow with a slightly reduced region of separation, and partially to thrust recovery. Based on the pressure coefficient curves previously discussed, flow entrainment appears minimal; the drag decrease is due mostly to thrust.
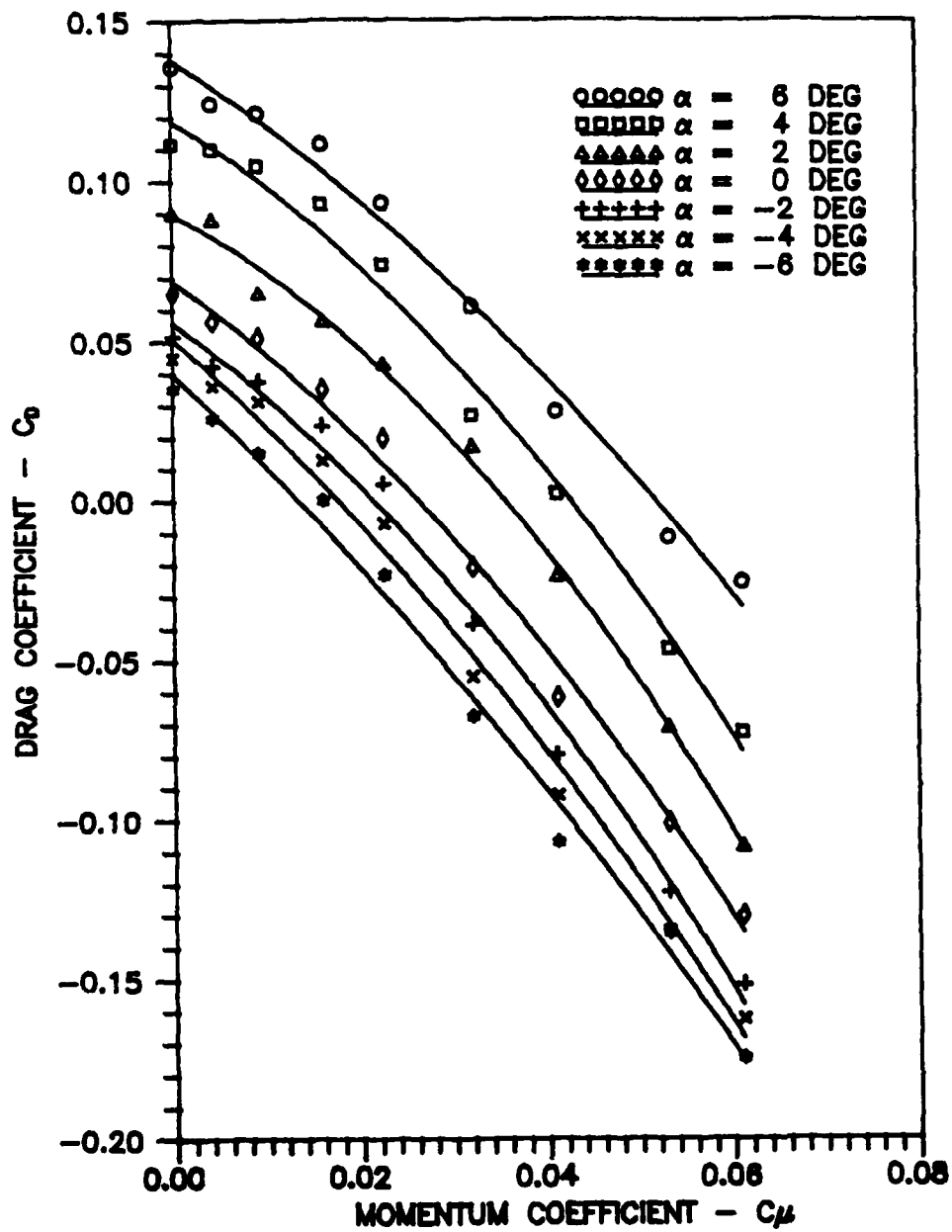
Figure 20. Drag as a Function of Momentum Coefficient, Re=9x10^{5}

Figure 21 is a plot of pitching moment coefficient as a function of momentum coefficient and angle of attack. Again, the trends exhibited are expected of a circulation control wing: increased blowing resulted in an increase of the nose-down moment. The production of a suction peak on the trailing edge, with a corresponding aft movement of the center of pressure, was partly responsible for this nose-down tendency. The jet thrust also contributed, as any jet turning cants the thrust vector upward, increasing the thrust moment arm to the leading edge. A comparison of these pitching moment results with the corresponding 2-D results is prohibitive, as the jet thrust effects were not included in the latter.

Equivalent drag results are presented in Figure 22. The equivalent drag curves are fairly typical of circulation control airfoils. An ever increasing penalty is paid as blowing is increased; the compressor power required to produce the jet flow is proportional to v_j^3 and rises fairly rapidly with momentum coefficient.

Care must be taken in comparing equivalent drag data from different sources, as these results can be presented in several forms. For example, some studies choose to neglect the ram inlet penalty. For the present case, comparison with the 2-D airfoil results shows somewhat higher values of equivalent drag for the wing. Aside from the obvious fact that 3-D models should generate higher drag, the 2-D model
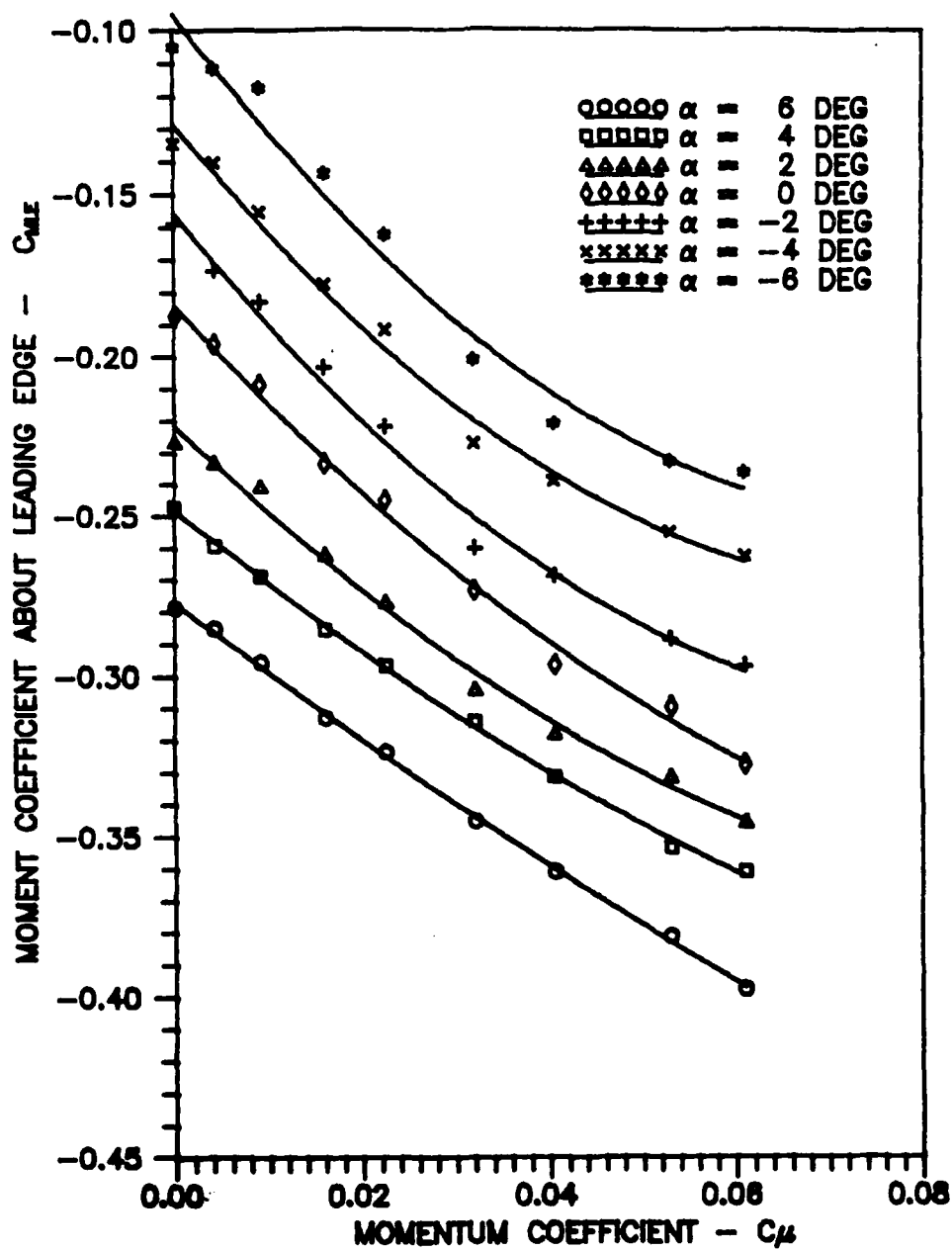
Figure 21.   Pitching Moment as a Function of Momentum
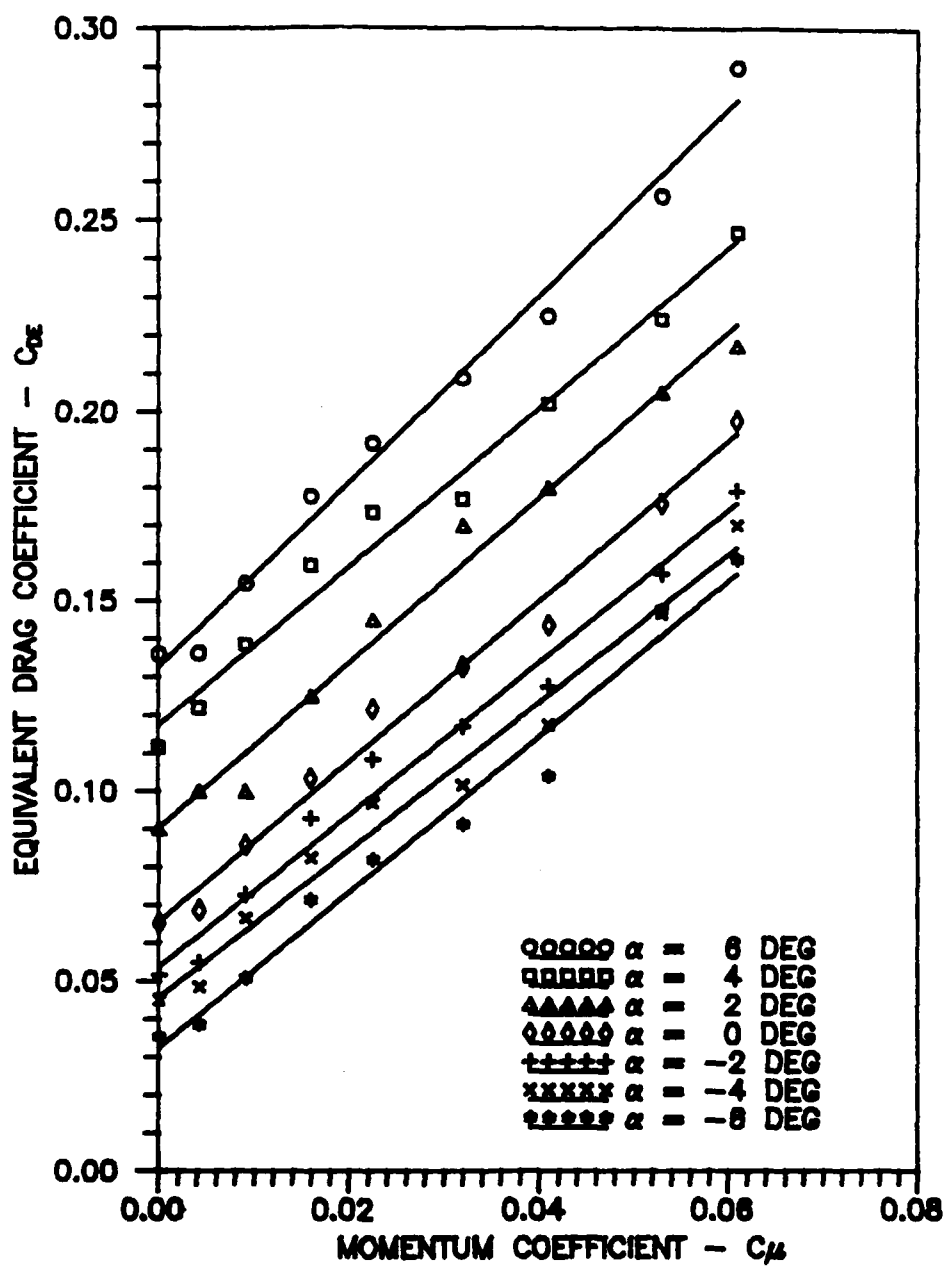   Coefficient, Re=9x10^5

Figure 22.   Equivalent Drag as a Function of Momentum
Coefficient, Re=9x10^5

produced more effective jet turning, with a smaller separation region and lower drag.

The lift-to-equivalent drag results of Figure 23 are very atypical of circulation control wings. Previous 2-D results indicate the efficiency (L/D_E) should increase to some maximum value before tapering off. The curves of Figure 23 unequivocally show that, especially at positive angles of attack, the equivalent drag penalty paid for blowing far outweighed any lift augmentation gained.

Finally, the flow visualization results indicate that the presence of the sting/hoses upstream of the trailing edge caused strong flow characteristics which influenced conditions at the trailing edge. Figure 24 is a sketch of the tufted wing upper surface as it appeared for any angle of attack or momentum coefficient tested. The upper surface flow was well behaved and attached up to the primary slot. However, the tufts reaching from the primary slot around the trailing edge showed very distinct spanwise turning in the mid-span region. Note that the outboard flow appeared quite straight and attached. Tufts on the lower surface trailing edge (not shown) turned slightly up and around the cylindrical aft surface, indicating some upwash near mid-span and agreeing with the pressure distribution curves presented earlier. From this tuft pattern, the lower surface flow is apparently curling up and around the hoses and sting, seeking out the low pressure region on the hose/sting opposite surfaces (recall the sting/hoses enter

53
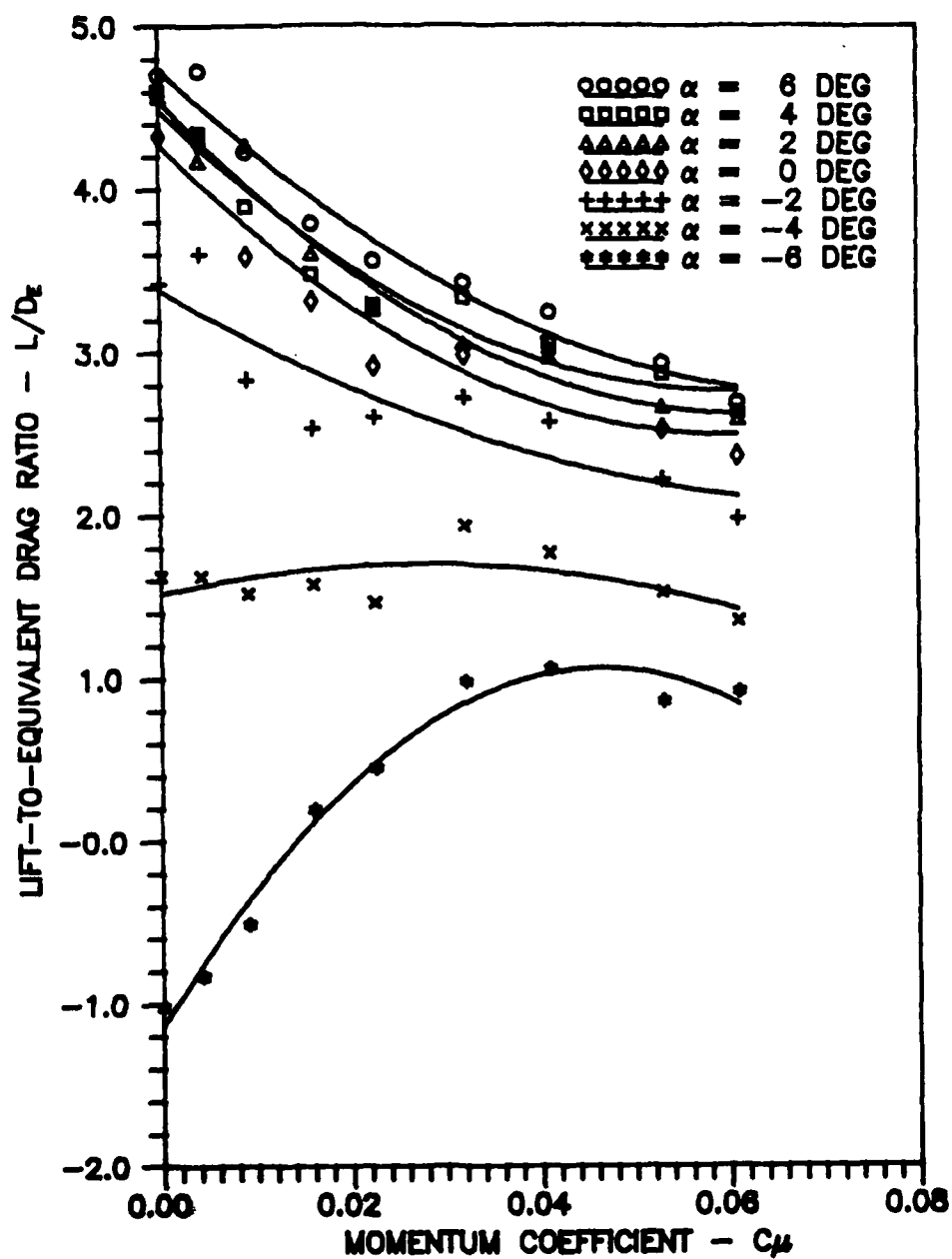
Figure 23. Lift-to-Equivalent Drag Ratio as a Function
of Momentum Coefficient, Re=9x10^5

the lower surface near mid-span at a 16 deg angle). The
upper surface flow followed this pattern, resulting in the
curved streamlines at the trailing edge. This flow
disturbance, possibly coupled with a weakness in the
trailing-edge/slot design (discussed earlier), appeared to
prevent strong jet attachment. Also, as blowing momentum
was considerably less than free-stream momentum, the jet was
unable to overcome this disturbance.

Removal of the air hoses reduced the region of flow
disturbance, but did not entirely eradicate it. The
presence of the sting alone caused similar flow disruption,
but to a lesser degree.
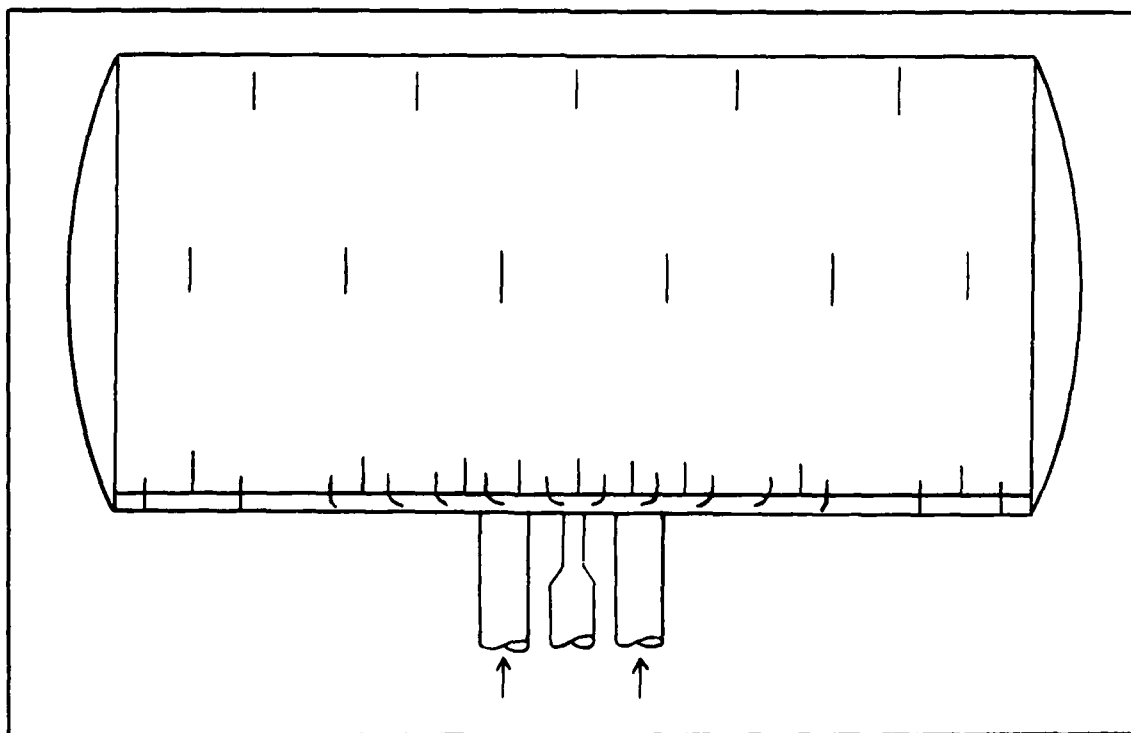
Figure 24. Tuft Pattern on Wing Upper Surface

$\underline{Re = 6 \times 10^5}$. The lift results of Figure 25 show slight improvements over earlier lift results, demonstrating a small, but noticeable, Reynolds number dependence. With the drop in free-stream dynamic pressure came a corresponding increase in momentum coefficient, leading to a stronger jet flow relative to free-stream. This added relative strength increased jet turning and circulation slightly, producing the greater lift coefficients.

The increase in ratio of jet thrust to aerodynamic drag, along with the slight circulation improvement, led to more negative values of both measured drag (Figure 26) and pitching moment (Figure 27).

An increase in momentum coefficient requires more compressor power. Therefore, with measured drag declining only slightly with Reynolds number, this increase in power required to produce the jet caused a corresponding increase in equivalent drag (Figure 28).

The lift-to-equivalent drag (wing efficiency) curves of Figure 29 present the combined effects of a small lift increase (higher momentum coefficient, improved jet turning) with an equivalent drag increase (more compressor power required). The lift increase was relatively small compared to the equivalent drag rise, causing efficiency to worsen with the Reynolds number drop.

The flow visualization runs at this Reynolds number exhibited the identical characteristics found previously, only to a somewhat lesser extent. Again, removal of the air
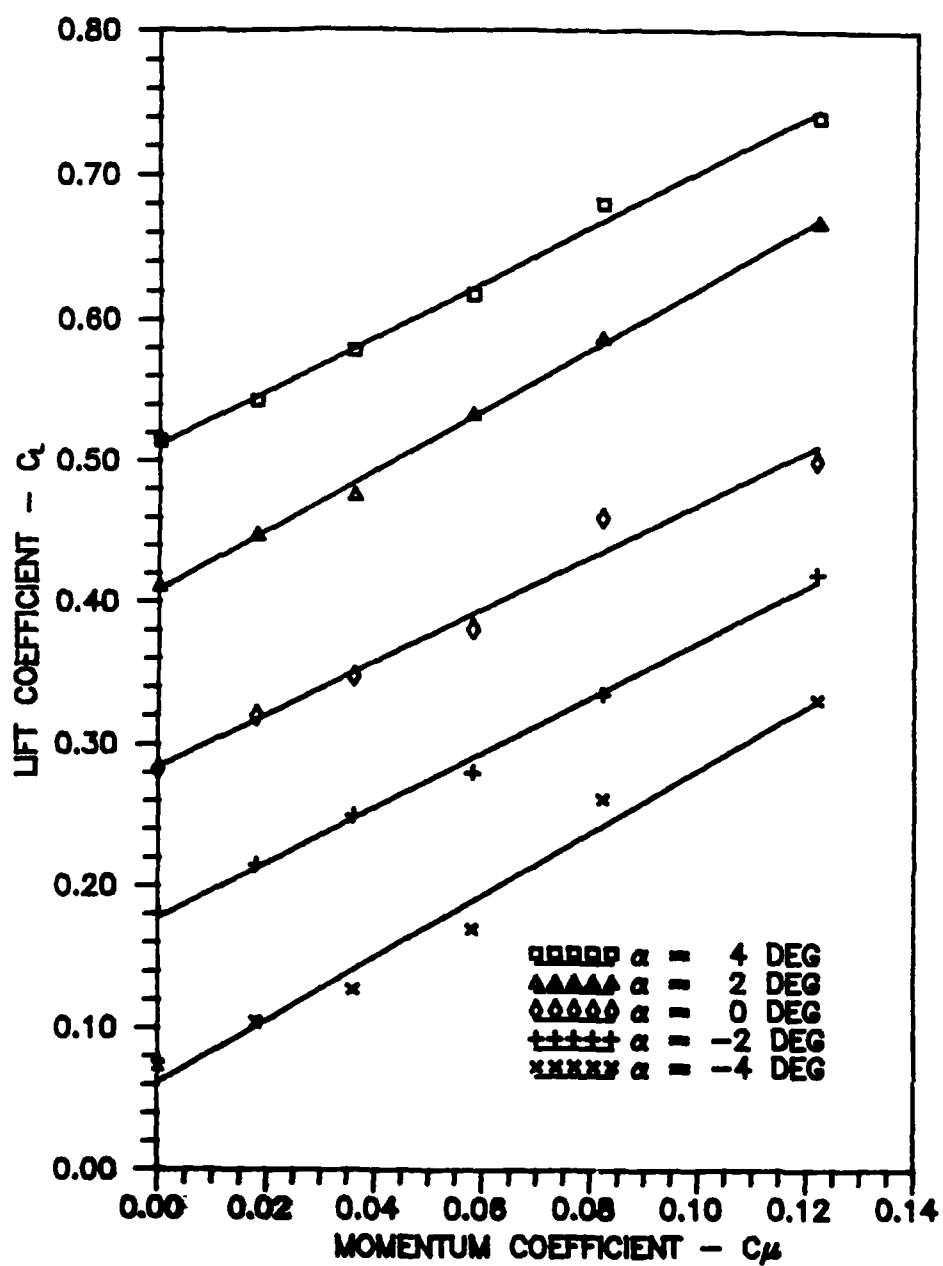
Figure 25.   Lift as a Function of Momentum Coefficient,
Re=6x10^5

57

Figure 26.   Drag as a Function of Momentum Coefficient, $Re=6x10^5$

58

Figure 27.   Pitching Moment as a Function of
              Momentum Coefficient, Re=6x10^5
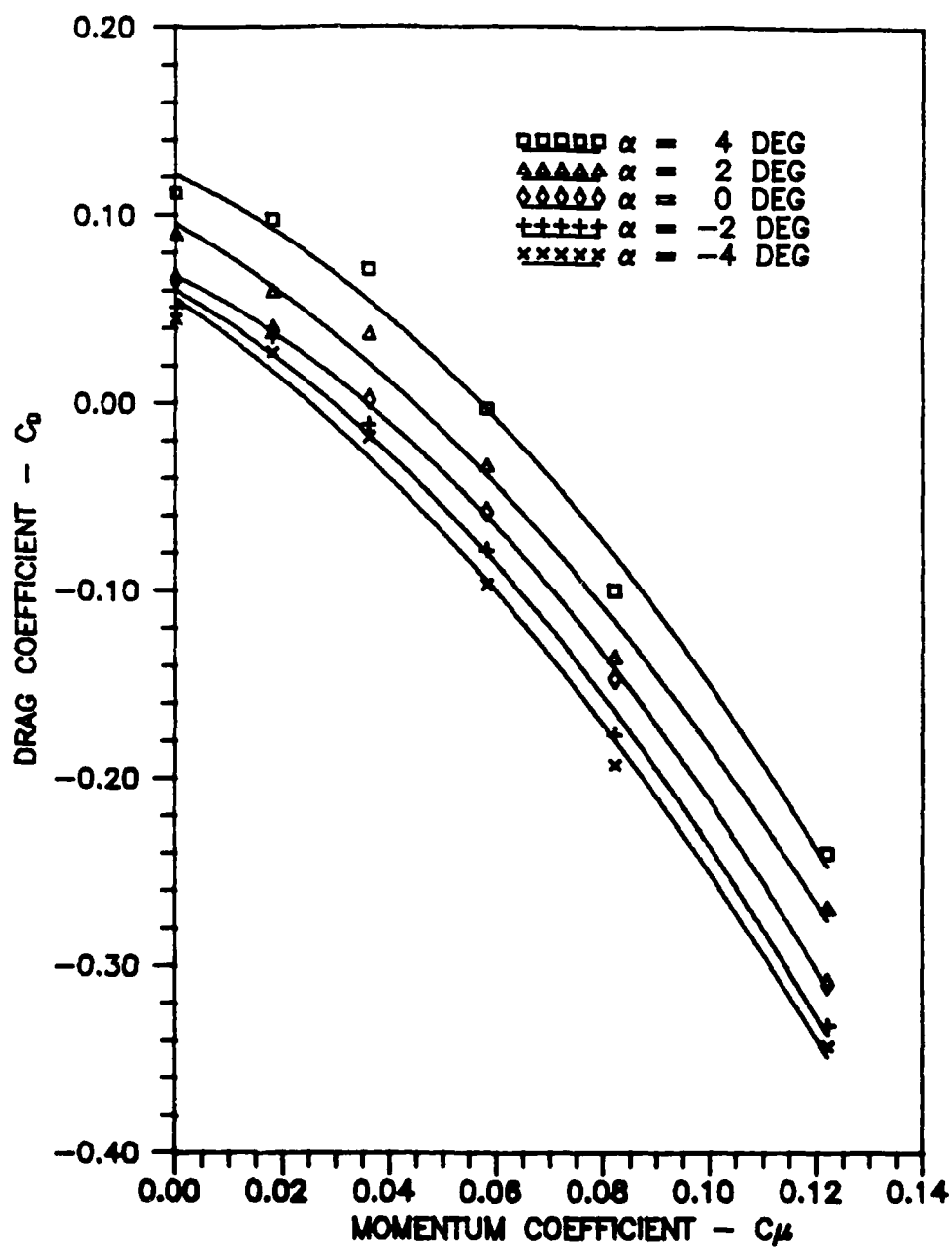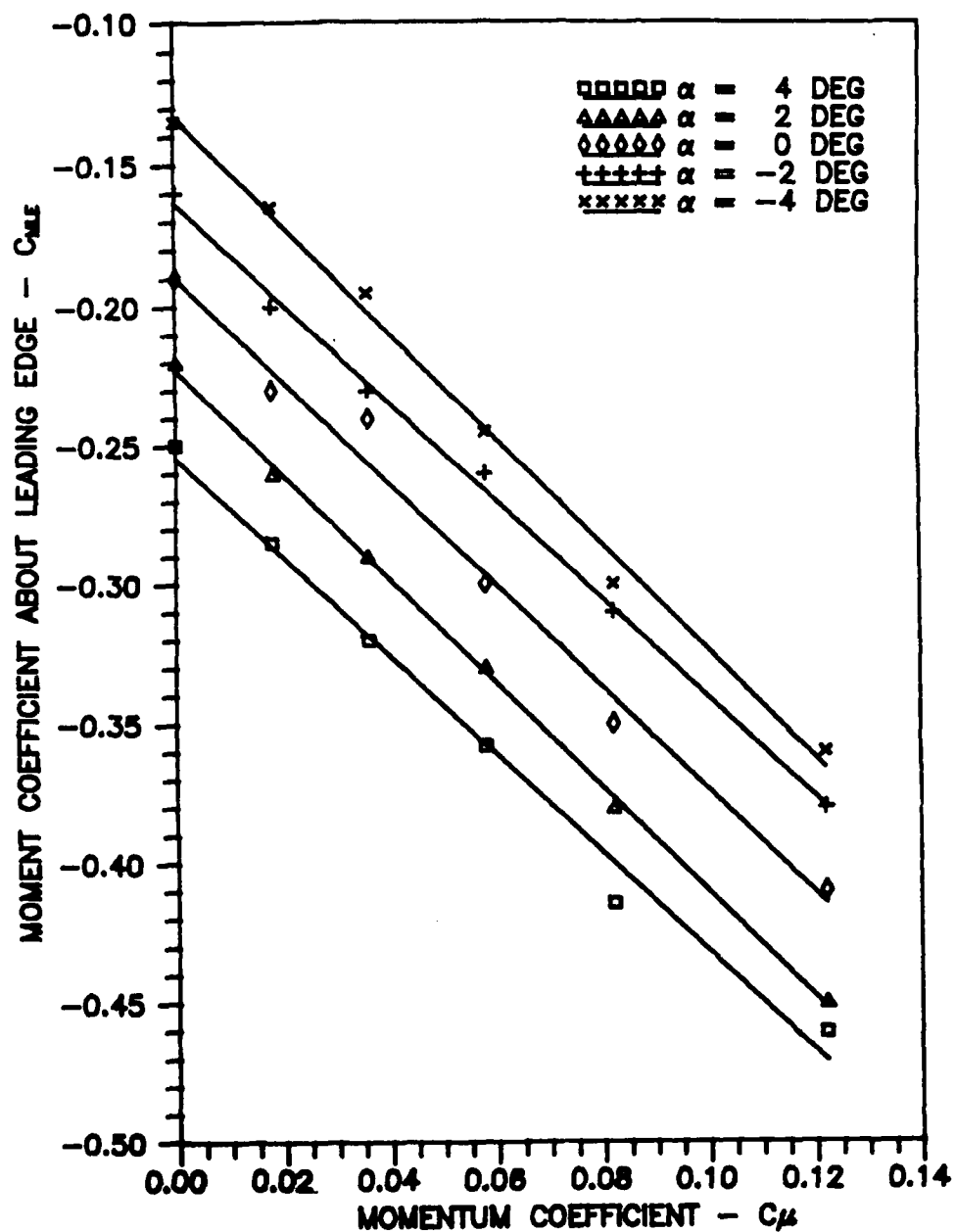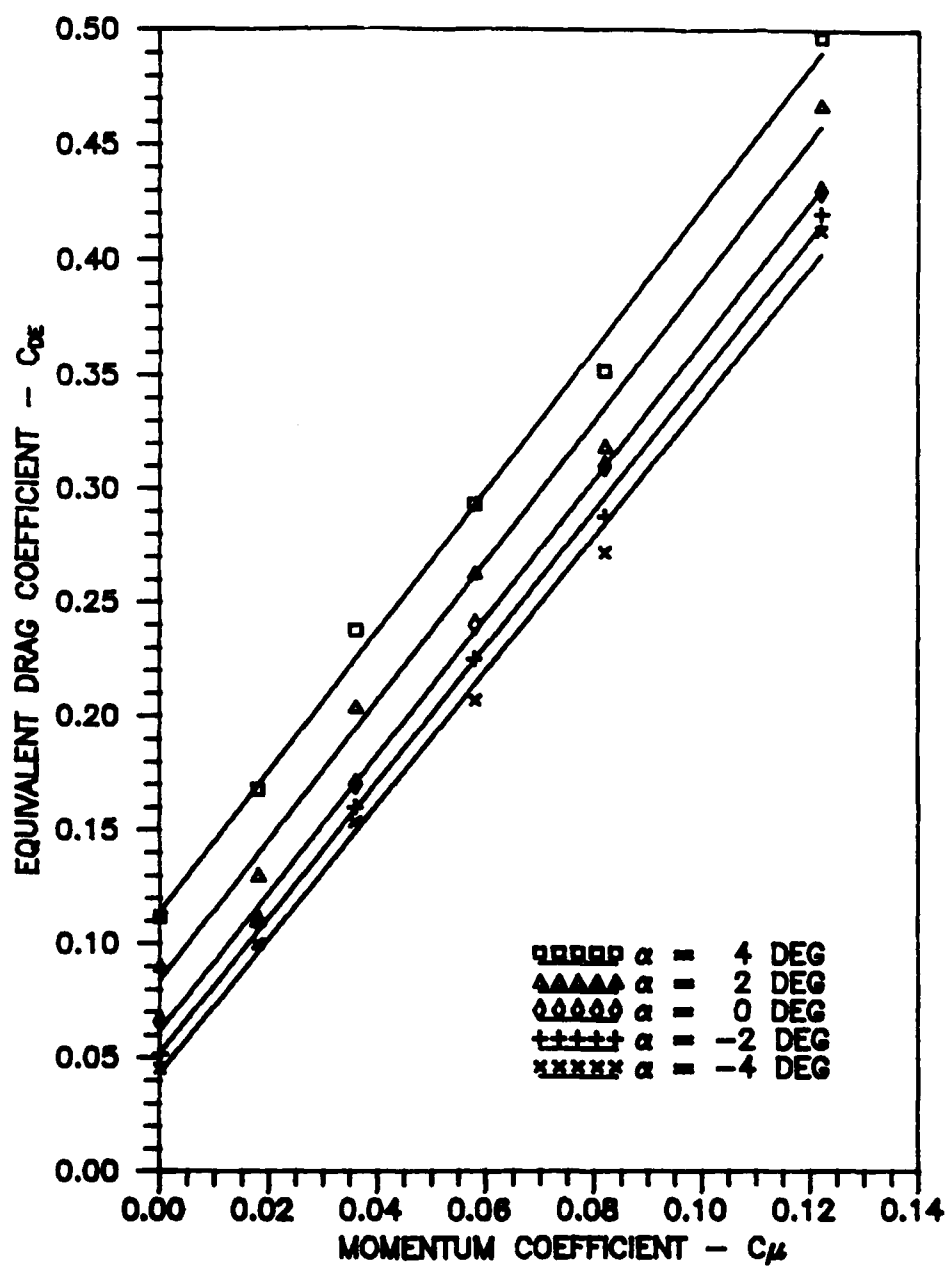
59

Figure 28. Equivalent Drag as a Function of
Momentum Coefficient, $Re=6x10^5$
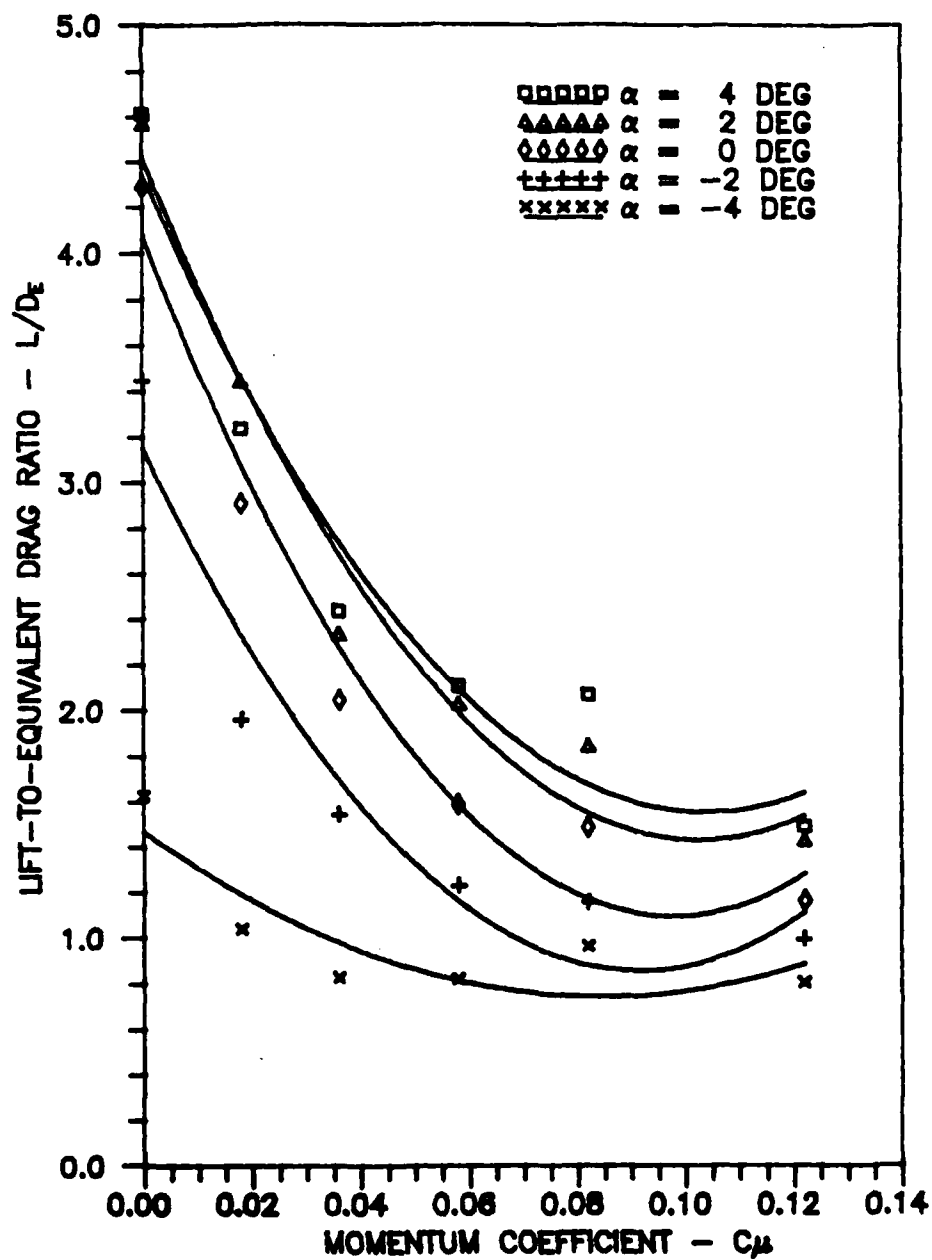
Figure 29. Lift-to-Equivalent Drag Ratio as a Function of Momentum Coefficient, Re=6x10^{5}

supply hoses revealed an improvement in the trailing-edge flow pattern.

Further Testing

Additional tests were accomplished in an attempt to correct the troublesome trailing-edge flow. First, check runs were made to ascertain whether jet impingement on the sting/hoses was adversely affecting the trailing-edge flow field. Four inches of the primary slot at mid-span was blocked; both force data runs and flow visualization runs were made. This affected neither the force data nor the tuft pattern. Next, 1-in. high vertical aluminum plates were attached to the wing lower surface, just outboard of the hoses, running fore and aft from the hose entrance to the trailing edge. The intent was to contain the region of flow disruption by preventing the mid-span lower surface flow (negotiating the sting/hoses) from corrupting the outboard flow. Force data and flow visualization runs were again conducted; test results showed no improvement. Finally, since jet momentum is proportional to v_j^2, boosting v_j could increase jet momentum enough to overcome the trailing-edge flow disruption. With this is mind, yet another modification was made on the primary slot, this time reducing the slot height to 0.010-in. Another tuft study of the primary-jet flow (tunnel off) indicated improved Coanda turning of approximately 90 deg, suggesting the smaller slot height improved initial jet attachment. Flow visualization runs at both test Reynolds numbers displayed a moderately

62

reduced region of flow disruption at higher blowing rates,
indicating the slot modification to be somewhat successful.
No force data was collected due to a force balance
malfunction.

VI. Conclusions

1. Overall, testing of this sting-mounted wing was found feasible if appropriate data corrections were made to account for the aerodynamic effects of the air supply hoses and the thrust effects of the jet. Repeatable data were obtained; results exhibit trends found in circulation control airfoil testing.

2. Lift augmentation was lower than anticipated, due to somewhat less jet turning than found during 2-D testing with the same airfoil section. Drag, equivalent drag, and pitching moment decreased (i.e., became more negative) with increased blowing, exhibiting trends common to circulation control airfoils. Lift-to-equivalent drag ratios were somewhat atypical; blowing was detrimental to wing efficiency. Reynolds number effects included better jet turning at lower Re, leading to slightly higher lift and more negative drag, equivalent drag, and pitching moment.

3. The wing design used in this study provided that the sting and two 1-in. air supply hoses enter the wing lower surface near mid-span, at a 16 deg angle with the chord line. This design detail, with the sting and hoses exposed to the free-stream upwind of the trailing edge, caused strong flow disturbances which hindered the blown jet from producing supercirculation. Placing the hoses on either

side of the sting, as opposed to above/below the sting, resulted in a relatively large spanwise region of flow disruption. Operationally, this suggests that wing pods, armament, etc. may severely limit blowing effectiveness on aircraft utilizing circulation control lifting surfaces.

4. The trailing-edge and slot geometry used, which required the jet to turn immediately upon exiting the slot, may have contributed to less-than-expected wing performance. In the presence of an adverse pressure gradient, such as that due to the flow disruption mentioned above, immediate jet attachment from this slot could be difficult.

VII. Recommendations

1. Since a force balance malfunction precluded data collection after the final slot modification, further test runs at both test Reynolds numbers should be carried out upon balance repair/replacement.

2. Further testing should be undertaken with a revised, single-slot model design. Limiting blowing to a single slot accomplishes two objectives. First, the need for a second air supply hose is eliminated, removing a source of flow disruption. Second, the cylindrical trailing edge would no longer contain a secondary plenum; the sting could enter the model through the trailing edge without concern for plenum integrity. This design also allows the sting/hose pair to enter the model parallel to the chord line instead of angled, further reducing free-stream disruption. The single air hose should be secured below the sting to contain the flow disturbance to as small a region as possible, with the air hose entering an aerodynamically faired "fuselage." Figure 30 is one such design.

3. Slight modifications to the slot geometry should be explored. A slight aft shift of the cylindrical trailing edge and an uppercut in the slot upper wall are recommended to improve jet attachment. Consideration should also be

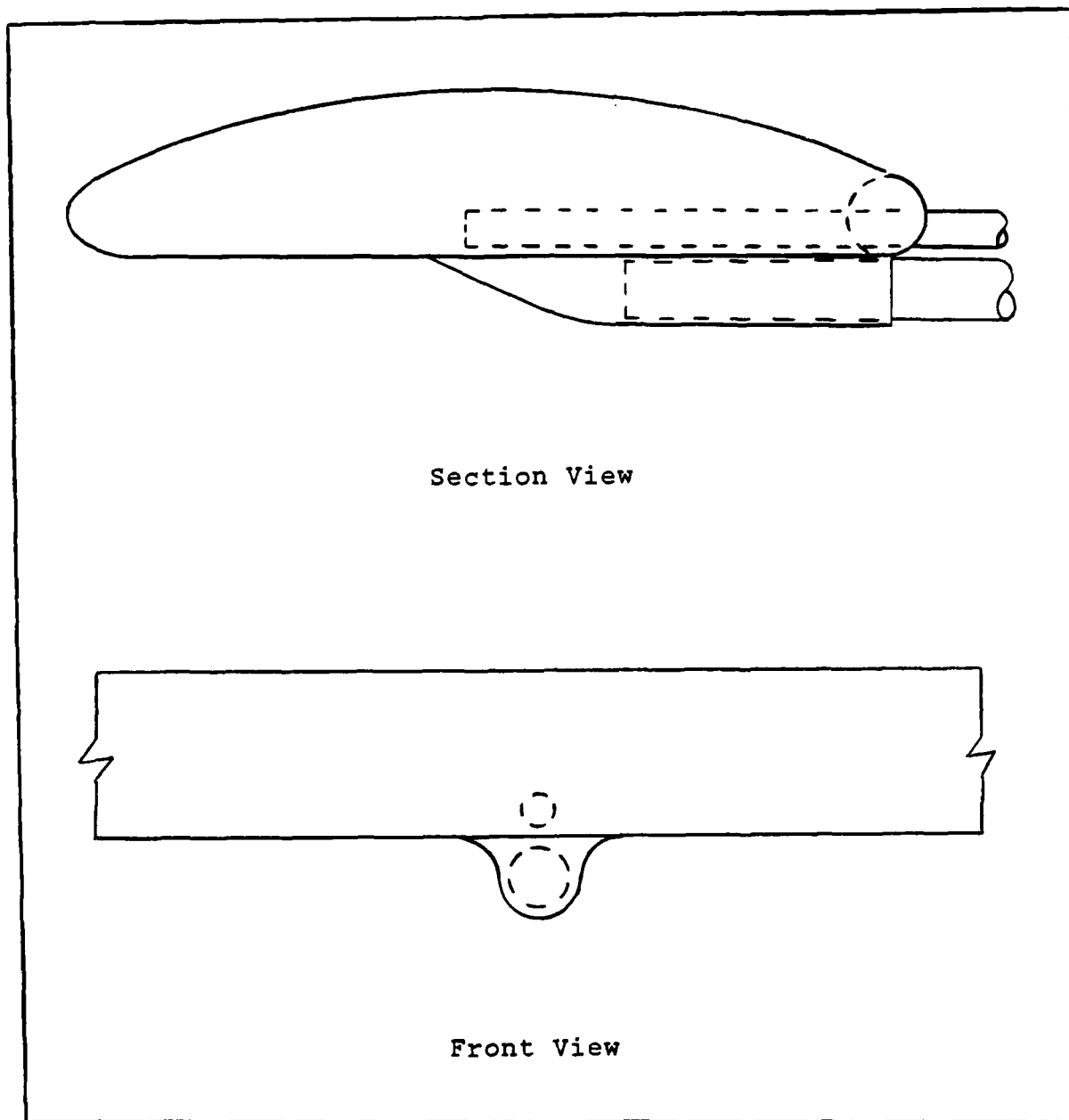Section View

Front View

Figure 30.   Recommended Single-Slot Wing Design

given to installing slot adjustment screws to facilitate
testing with several slot heights.   An investigation into a
slot height/wing performance correlation is warranted.

Bibliography

1. Englar, R. J. <u>Experimental Investigation of the High Velocity Coanda Wall Jet Applied to Bluff Trailing Edge Circulation Control Airfoils</u>. NSRDC Technical Report 4708. Bethesda MD: Naval Ship Research and Development Center, September 1975.

2. Harvell, J. K. and Franke, M. E. "Aerodynamic Characteristics of a Circulation Control Airfoil with Two Blown Slots, "<u>Journal of Aircraft</u>, 22: 737-742 (September 1985).

3. Kind, R. J. and D. J. Maull. "An Experimental Investigation of a Low-Speed Circulation-Controlled Aerofoil, " <u>The Aeronautical Quarterly</u>, 19: 170-182 (May 1968).

4. Englar, R. J. <u>Two-Dimensional Subsonic Wind Tunnel Tests of Two 15-Percent Thick Circulation Control Airfoils</u>. NSRDC Technical Note AL-211. Bethesda, MD: Naval Ship Research and Development Center, August 1971.

5. Williams, R. M. and H. J. Howe. <u>Two-Dimensional Subsonic Wind Tunnel Tests on a 20-Percent Thick, 5-Percent Cambered Circulation Control Airfoil</u>. NSRDC Technical Note AL-176. Bethesda, MD: Naval Ship Research and Development Center, August 1970.

6. Abramson, J. <u>Two-Dimensional Subsonic Wind Tunnel Evaluation of a 20-Percent Thick Circulation Control Airfoil</u>. DTNSRDC Technical Report ASED-331. Bethesda, MD: David Taylor Naval Ship Research and Development Center, Code 1619, June 1975.

7. Loth, J. L. et al. "Flight Performance of a Circulation Controlled STOL Aircraft," <u>Journal of Aircraft</u>, 13:169-173 (March 1976).

8. Englar, R. J. <u>Development of the A-6/Circulation Control Wing Flight Demonstrator Configuration</u>. DTNSRDC Technical Report ASED 79/01. Bethesda, MD: David Taylor Naval Ship Research and Development Center, Code 1619, January 1979.

9. Franke, M. E. and J. K. Harvell. "Wind Tunnel Studies of Circulation Control Elliptical Airfoils," <u>Proceedings of the Circulation-Control Workshop 1986</u>, 267-287. Moffett Field, CA: NASA Ames Research Center, February 1986.

10. Williams, Steven L. <u>Use of Navier-Stokes Methods to Predict Circulation Control Airfoil Performance</u>. MS thesis, AFIT/GAE/AA/89M-4. School of Engineering, Air Force Institute of Technology (AU), Wright-Patterson AFB OH, March 1989.

11. NASA Ames Research Center. <u>Proceedings of the Circulation-Control Workshop 1986</u>. NASA Conference Publication 2432. Moffett Field, CA: February 1986.

12. Harvell, Capt John K. <u>An Experimental/Analytical Investigation into the Performance of a 20-Percent Thick, 8.5-Percent Cambered Circulation Controlled Airfoil</u>. MS thesis, AFIT/GAE/AA/82D-13. School of Engineering, Air Force Institute of Technology (AU), Wright-Pa'terson AFB OH, December 1982 (AD-A124732).

13. Walters, R. E. et al. <u>Circulation Control By Steady and Pulsed Blowing for a Cambered Elliptical Airfoil</u>. Contract N00014-68-A-0512. Morgantown, WV: West Virginia University, 1972 (AD-751045).

14. Wood, N. and J. Nielsen. <u>Circulation Control Airfoils Past, Present, Future</u>. AIAA Paper 85-0204. American Institute of Aeronautics and Astronautics, January 1985.

15. Englar, R. J. <u>Low-Speed Aerodynamic Characteristics of a Small, Fixed-Trailing-Edge Circulation Control Wing Configuration Fitted to a Supercritical Airfoil</u>. DTNSRDC Technical Report ASED-81/08. Bethesda, MD: David Taylor Naval Ship Research and Development Center, March 1981.

16. Shames, Irving H. <u>Mechanics of Fluids</u>. New York: McGraw-Hill, Inc., 1982.

17. Pope, A. and W. H. Rae. <u>Low-Speed Wind Tunnel Testing</u>. New York: John Wiley & Sons, Inc., 1984.

18. Roskam, J. <u>Airplane Flight Dynamics and Automatic Flight Controls: Part I</u>. Ottawa: Roskam Aviation and Engineering Corp., 1979.

19. Systems Research Laboratories. <u>AFIT 5-ft Wind Tunnel Data Acquisition System</u>. Version 1.1, User's Manual. Wright-Patterson AFB, January 1989.

20. Pressure Systems, Inc. <u>Model 780B/T Pressure Measurement System Users Manual</u>. First Edition, September 1983.

21. Englar, R. J. <u>Test Techniques for High-Lift, Two-Dimensional Airfoils with Boundary Layer and Circulation Control for Application to Rotary Wing Aircraft</u>. NSRDC Technical Report 4645. Bethesda, MD: Naval Ship Research and Development Center, July 1975.

22. Bertin, J. and M. Smith. <u>Aerodynamics For Engineers</u>. Englewood Cliffs NJ: Prentice-Hall, 1979.

Vita

Captain John W. Trainor ████████████████████████
████████████████████████ He graduated from Greely High
School in Cumberland, Maine, in 1981 and began attending
Virginia Tech. In 1985 he graduated with a degree of
Bachelor of Science in Aerospace & Ocean Engineering. He
was commissioned in September 1985 upon graduation from
Officer Training School at Lackland AFB, Texas. From
September 1985 to May 1988 he served as a project manager
with the 4484 Test Squadron, Tactical Air Warfare Center, at
Tyndall AFB, Florida. In May 1988 Captain Trainor
transferred to the School of Engineering, Air Force
Institute of Technology, Wright-Patterson AFB, Ohio.

REPORT DOCUMENTATION PAGE

Form Approved
OMB No. 0704-0188

1a. REPORT SECURITY CLASSIFICATION UNCLASSIFIED	1b. RESTRICTIVE MARKINGS		
2a. SECURITY CLASSIFICATION AUTHORITY	3. DISTRIBUTION/AVAILABILITY OF REPORT		
2b. DECLASSIFICATION/DOWNGRADING SCHEDULE	Approved for public release; distribution unlimited.		
4. PERFORMING ORGANIZATION REPORT NUMBER(S) AFIT/GAE/ENY/89D-38	5. MONITORING ORGANIZATION REPORT NUMBER(S)		

6a. NAME OF PERFORMING ORGANIZATION School of Engineering	6b. OFFICE SYMBOL (If applicable) AFIT/ENY	7a. NAME OF MONITORING ORGANIZATION
6c. ADDRESS (City, State, and ZIP Code) Air Force Institute of Technology (AU) Wright-Patterson AFB, OH 45433-6583		7b. ADDRESS (City, State, and ZIP Code)

8a. NAME OF FUNDING/SPONSORING ORGANIZATION	8b. OFFICE SYMBOL (If applicable)	9. PROCUREMENT INSTRUMENT IDENTIFICATION NUMBER

8c. ADDRESS (City, State, and ZIP Code)	10. SOURCE OF FUNDING NUMBERS			
	PROGRAM ELEMENT NO.	PROJECT NO.	TASK NO	WORK UNIT ACCESSION NO.

11. TITLE (Include Security Classification)
A WIND TUNNEL STUDY OF A STING-MOUNTED CIRCULATION CONTROL WING

12. PERSONAL AUTHOR(S)
John W. Trainor, Capt, USAF

13a. TYPE OF REPORT MS Thesis	13b. TIME COVERED FROM _____ TO _____	14. DATE OF REPORT (Year, Month, Day)]989 December	15. PAGE COUNT 85

16. SUPPLEMENTARY NOTATION

17. COSATI CODES			18. SUBJECT TERMS (Continue on reverse if necessary and identify by block number)
FIELD	GROUP	SUB-GROUP	Wind Tunnel Test Short-Takeoff Aircraft
0]	0]		Wing Circulation Control
01	03	07	

19. ABSTRACT (Continue on reverse if necessary and identify by block number)

Thesis Advisor: Dr. Milton E. Franke
Professor of Aerospace Engineering
Dept. of Aeronautics and Astronautics

20. DISTRIBUTION/AVAILABILITY OF ABSTRACT ☑ UNCLASSIFIED/UNLIMITED ☐ SAME AS RPT. ☐ DTIC USERS	21. ABSTRACT SECURITY CLASSIFICATION UNCLASSIFIED	
22a. NAME OF RESPONSIBLE INDIVIDUAL Dr. Milton E. Franke	22b. TELEPHONE (Include Area Code) 5]3-255-2362	22c. OFFICE SYMBOL AFIT/ENY

DD Form 1473, JUN 86   Previous editions are obsolete.   SECURITY CLASSIFICATION OF THIS PAGE

Abstract

This wind tunnel study investigated the feasibility of testing a sting mounted circulation control wing. A 20% thick, 8.5% cambered rectangular wing was designed, built, and tested in the AFIT 5-ft wind tunnel. Lift, drag, equivalent drag, and pitching moment coefficients were obtained at Reynolds numbers of $6x10^5$ and $9x10^5$. The force and moment results achieved indicate supercirculation was not present. Flow visualization with nylon tufts displayed extreme flow disruption at the trailing edge, due to free-stream impingement on both the sting and blowing air supply hoses. The available blowing air supply was not strong enough to produce a jet flow with the momentum needed to overcome this disruption. Wing model design changes were recommended to alleviate this problem.